Hepatitis C virus induces HuR relocalization by coordinating PKC-δ and AMPK-α function

Harsha Raheja[1], Biju George[1], Sandhini Saha[2], Saurav Malik[1], Tushar Kanti Maiti[2], Saumitra Das[1*]

1. Department of Microbiology and Cell Biology, Indian Institute of Science, Bangalore-560012

2. Regional Centre for Biotechnology, Faridabad

Running title: HCV-induced HuR translocation mechanism

* To whom correspondence should be addressed.

Prof. Saumitra Das

Department of Microbiology and Cell Biology

Indian Institute of Science, Bangalore-560012, India

Phone: +91 80 2293 2886, Fax: +91 80 2360 2697

Email: sdas@iisc.ac.in

Abstract

Host protein HuR translocation from nucleus to cytoplasm following infection is crucial for the life cycle of several RNA viruses including hepatitis C virus (HCV), a major causative agent of hepatocellular carcinoma. HuR assists the assembly of replication-complex on the viral-3′UTR, and its depletion hampers viral replication. Although cytoplasmic HuR is crucial for HCV life cycle, little is known about the mechanism of its translocation. We show that the viral protein NS3 activates protein kinase C (PKC)-δ, which in-turn phosphorylates HuR on S318 residue, triggering its export to the cytoplasm. The mechanism of retention of translocated HuR in cytoplasm was further studied. HCV protein NS5A reduces AMP-activated kinase (AMPK) activity in the cytoplasm, thereby preventing AMPK-mediated phosphorylation and acetylation of importin-α1, the nuclear carrier of HuR. The resulting increased retention of HuR in cytoplasm was reversed by treatment of cells with an AMPK activator. Our results show that viral NS3 and NS5A proteins orchestrate two different cellular kinases, PKC-δ and AMPK, to determine the cytoplasmic availability of HuR, to regulate HCV life cycle and pathogenesis.

Keywords: Hepatitis C virus/ HuR translocation/ HuR phosphorylation/ PKC-δ in virus infection/ AMPK in virus infection

Introduction

Hepatitis C virus (HCV) is an RNA virus, whose 9.6-kb genome codes for three structural and seven non-structural proteins (Lindenbach & Rice, 2005). Structural proteins form the viral capsid and envelope, whereas non-structural proteins are involved in the regulation of various viral life processes, including double-membrane vesicle formation, replication, translation, packaging, and release (Dentzer, Lorenz et al., 2009, Gu & Rice, 2013, Jirasko, Montserret et al., 2010, Ray & Das, 2011). The viral open reading frame is flanked by two

43 regulatory elements, the 5'-untranslated region (UTR) and 3'-UTR, which are involved in
44 initiating viral translation and replication, respectively (Gu & Rice, 2013).

45 Multiple host factors are required at various stages of the viral life cycle. Upon viral
46 infection, proteins, such as some IRES trans-acting factors and Nups relocate from the
47 nucleus to the cytoplasm to regulate the viral life cycle (Bonamassa, Ciccarese et al., 2015,
48 Niepmann & Gerresheim, 2020, Sharma, Raheja et al., 2018). Our laboratory has previously
49 shown that human antigen R (HuR), also known as ELAVL1, relocates from nucleus to the
50 cytoplasm upon HCV infection. HuR binds to the viral 3'-UTR, where it displaces the
51 replication inhibitor protein PTB and assists in the binding of the La protein. La further
52 recruits the entire replication complex to initiate viral replication (Shwetha, Kumar et al.,
53 2015). HuR is an RNA-binding protein (RBP), that shuttles between nucleus and cytoplasm.
54 Its endogenous function is to regulate the transport, stability, and translation of cellular RNAs
55 (Ma, Cheng et al., 1996, Schultz, Preet et al., 2020, Srikantan & Gorospe, 2012). Infection-
56 induced relocalization of HuR to the cytoplasm is required for interaction with viral RNA,
57 which guides viral replication. In a genome wide CRISPR screen, HuR was identified as a
58 major host factor required for HCV replication and the specific knockout was found to
59 abolish the HCV RNA replication in cells (Marceau, Puschnik et al., 2016).

60 HuR contains three RNA recognition motifs (RRMs) and a hinge region, also known as the
61 HuR nuclear shuttling domain (HNS domain) (Fan & Steitz, 1998, Fialcowitz-White, Brewer
62 et al., 2007, Ripin, Boudet et al., 2019). Phosphorylation of HuR residues regulates its
63 structure, RNA-binding affinity, and subcellular localization (Grammatikakis, Abdelmohsen
64 et al., 2017). HuR is phosphorylated in a cell-cycle dependent manner by CDKs. CDK1
65 phosphorylates HuR on S202, which is required for its nuclear retention during the S and G2
66 phases of the cell cycle (Kim, Abdelmohsen et al., 2008). Phosphorylation on the same site
67 by CDK5 has been shown to reduce its binding to cyclin A mRNA, leading to cell cycle

68 arrest in glioma cells (Filippova, Yang et al., 2012). Checkpoint kinase 2 (CHK2)
69 phosphorylates HuR on S88, S100, and T118, which modulates HuR binding to RNA by
70 decreasing its affinity for certain mRNAs (e.g., SIRT1) and increasing it for others (e.g., Myc
71 and occludin) (Abdelmohsen, Pullmann et al., 2007). Phosphorylation on S242 augments the
72 amount of HuR in the cytoplasm, regardless of stress conditions such as exposure to short-
73 wavelength ultraviolet light (Kim, Yang et al., 2008). The MAP kinase p38, which is
74 activated during inflammatory response, phosphorylates HuR on T118, increasing its binding
75 to and the stabilization of inflammatory mRNAs, such as p21, COX2, and $cPLA_2\alpha$, in
76 addition to promoting HuR accumulation in the cytoplasm (Lafarga, Cuadrado et al., 2009,
77 Liao, Wang et al., 2011). Several members of the protein kinase C (PKC) family are also
78 involved in HuR phosphorylation. PKC-α phosphorylates HuR on S158 and S221, which
79 leads to its cytoplasmic relocalization and enhanced binding to targets, such as COX2 and
80 PTGS2 (Doller, Huwiler et al., 2007). PKC-δ-mediated phosphorylation on S318 and S221
81 has been shown to induce cytoplasmic translocation and increased binding to COX2,
82 CCNDA2, and CCND1 mRNAs (Doller, Akool el et al., 2008, Doller, Schlepckow et al.,
83 2010). Abrogation of phosphorylation on S318 hinders the migration and invasion of colon
84 cancer cells (Doller, Winkler et al., 2011). Other kinases, such as IKKα, ERK8, and JAK3,
85 also phosphorylate HuR to regulate its localization and function (Chu, Chuang et al., 2012,
86 Liwak-Muir, Dobson et al., 2016, Yoon, Abdelmohsen et al., 2014). Activated JAK3
87 phosphorylates HuR on Y200, which prevents its inclusion in stress granules formed upon
88 arsenic treatment (Yoon et al., 2014). Phosphorylation of Y5, Y95, Y105, and Y200 residues
89 by SRC and ABL1 kinases is important for centrosomal accumulation of HuR and, therefore,
90 genomic stability (Filippova, Yang et al., 2015). In addition to phosphorylation, HuR is
91 methylated on R217 by CARM1, which correlates with its cytoplasmic localization in non-
92 small cell lung carcinoma (Vigouroux, Casse et al., 2015). Ubiquitination on K313 and K326

93 leads to the dissociation of HuR from p21, MKP1, and SIRT1 mRNA (Zhou, Geng et al.,
94 2013); whereas neddylation on K283, K313, and K326 promotes nuclear localization and
95 protein stability (de Sousa, Lima Mde et al., 2015).

96 Subcellular localization of HuR is also regulated by AMP-activated kinase (AMPK) (Wang,
97 Fan et al., 2002). Inhibition of AMPK has been associated with cytoplasmic localization of
98 HuR, leading to increased stability of the HuR-bound transcripts p21, cyclin B1, cyclin A,
99 and IL-20. AMPK phosphorylates importin-α1 on S105 and acetylates it on K22, thereby
100 preventing its interaction with HuR and import to the nucleus (Wang, Yang et al., 2004).

101 Cells adopt multiple strategies to regulate the subcellular localization of HuR and,
102 consequently, the stability of its cognate transcripts under different conditions. Here, we
103 investigated the viral mechanism driving the nuclear export of HuR, the cytoplasmic
104 partitioning of HuR, and the effect of its altered localization. We report that PKC-δ and
105 AMPK work in a coordinated manner to achieve cytoplasmic localization of HuR via direct
106 modification and indirect regulation of its nuclear carrier. Thus, HCV modulates two separate
107 kinases to promote replication and pathogenesis. Relocalization of HuR and its interaction
108 with cytoplasmic RNAs could reveal the molecular basis of HCV-induced hepatocellular
109 carcinoma and provide an attractive target for preventing its progression.

110 **Results**

111 **Phosphorylation of HuR regulates its cellular localization upon HCV infection**

112 Viruses are known to modify host proteins (Kumar, Mehta et al., 2020). To study the post-
113 translational modifications of host proteins after HCV infection, total protein extracts
114 prepared from mock (control) and HCV-RNA transfected Huh7.5 cells were analyzed by
115 two-dimensional gel electrophoresis and HuR-specific spots were detected using anti-HuR
116 antibody. In control cells, two spots were observed for HuR, one at the acidic end towards pH

117 3 and the other at the basic end towards pH 10. The spots had the same molecular weight,
118 suggesting the presence of two sub-populations of HuR with separate charged modifications
119 that did not alter overall protein weight. An additional spot, slightly more acidic than the one
120 at pH 10 (marked with an asterisk in Fig 1A), was observed upon HCV infection (Fig 1A, B),
121 indicating a negatively charged modification on HuR.

122 Phosphorylation is a post-translational modification that imparts a negative charge on
123 proteins. Therefore, we examined the involvement of phosphorylation on HuR following
124 HCV infection. Some phosphorylation sites known to impact HuR subcellular localization
125 include T118, Y200, S221, S242, and S318. The phospho-dead mutants of these sites were
126 generated using site-directed mutagenesis, wherein the serine or threonine residues were
127 replaced by alanine (T118A, S221A, S242A, S318A), and tyrosine was replaced by
128 phenylalanine (Y200F). The mutants were verified by sequencing and employed in the
129 relocalization assay. Endogenous HuR translocates from the nucleus to the cytoplasm 48h
130 after HCV-RNA transfection (Shwetha et al., 2015). If phosphorylation of a particular residue
131 is crucial for guiding this translocation, the corresponding phospho-dead mutant would
132 prevent the cytoplasmic relocalization of the mutant protein upon viral infection. Wild-type
133 (WT) HuR overexpression was used as a positive control for HuR localization. Using
134 immunostaining, the subcellular localization of WT and mutant HuR proteins was detected in
135 uninfected control and HCV-infected cells. Myc-tagged WT and mutant HuR was
136 overexpressed in Huh7.5 cells, followed by HCV-RNA transfection (Fig 1C). An anti-Myc-
137 tag antibody was used to visualize the overexpressed protein, the HCV Core protein was used
138 to identify HCV-infected cells, and DAPI was used to mark the nuclei. In untransfected
139 control cells, WT and all mutant HuR proteins localized to the nucleus (Fig 1D, E). HCV-
140 RNA transfection led to the relocalization of WT HuR to the cytoplasm. The same was
141 observed for HuR mutants S221A and S242A. Instead, mutants S318A, Y200F, and T118A

142 localized to the nucleus even after 48h of HCV-RNA transfection (Fig 1F, G). This finding
143 suggests that phosphorylation of S318, Y200, and T118 might be involved in relocalization
144 of HuR to the cytoplasm upon HCV infection.

145 **HuR is differentially phosphorylated upon HCV infection**

146 To validate HCV induced HuR phosphorylation, total phosphorylated proteins were
147 immunoprecipitated using pan-anti-phospho-Ser/Thr and pan-anti-phospho-Tyr antibodies.
148 The presence of HuR in the pull-down fraction of both antibodies confirmed HuR
149 phosphorylation in cells (Fig 2A, B). To identify the phosphorylation sites on HuR, the latter
150 was immunoprecipitated from control or HCV-RNA-transfected cells, and the pull-down
151 fraction was subjected to mass-spectrometric analysis (Fig 2C, D). The results revealed six
152 previously characterized sites, including T80, S88, T143, S146, S202, and S318, as well as
153 two new sites, S135 and T293 (Fig 2E). The abundance of phosphorylated peptides at a
154 particular site was calculated as the fraction of phosphorylated peptides to total peptides
155 observed for that site. Quantification was performed for S318, which was previously found to
156 be regulated by HCV infection, as well as for S202, which is known to regulate HuR
157 localization, and S135, which has not yet been characterized. The percentage of
158 phosphorylated S318 increased in all three sets of HCV-RNA transfected cells compared to
159 control cells (Fig 2F). S202 phosphorylation varied among separate sets of experiments (Fig
160 2G); whereas S135 phosphorylation was reduced upon HCV-RNA transfection in all three
161 sets (Fig 2H). Differential phosphorylation at distinct HuR sites might explain the absence of
162 an overall variation (Fig 2A, B). Because S318 phosphorylation was higher following HCV
163 infection and was found to be important for HuR relocalization (Fig 1F,G), this site was
164 selected for further studies.

165 **Phosphorylation of S318 influences HCV replication**

166 The location of the S318 site on HuR was visualized using Pymol software. The X-ray
167 structure of HuR RRM3 (PDB ID: 6GD2) complexed with RNA indicated that the S318 site
168 was on the surface of the protein and interacted directly with the bound RNA (Fig 3A).
169 Accordingly, phosphorylation of S318 might affect the RNA binding of HuR. To study the
170 impact of phosphorylation on the affinity for HCV-RNA, we used surface plasmon
171 resonance. Biotinylated HCV 3'-UTR RNA was immobilized on a streptavidin-coated SPR
172 chip (SA Chip) and recombinant purified WT, S318A, and S318D HuR proteins were passed
173 over as analytes to calculate the binding affinity (Fig 3B–D). The Kd values for WT and
174 S318A HuR were 25.7 nM and 46.2 nM, respectively; whereas the phospho-mimic mutant
175 S318D showed approximately five-fold better affinity (Kd 6.36 nM) (Fig 3E). This result
176 indicates that, along with relocalization to the cytoplasm, S318 phosphorylation of HuR also
177 augments the binding affinity for HCV 3'-UTR. To assess the impact of S318
178 phosphorylation on HCV replication, WT, S318A, and S318D constructs were overexpressed
179 in Huh7.5 cells, followed by HCV-RNA transfection (Fig 3F). The effect on replication was
180 checked by analyzing the levels of HCV negative-strand RNA compared to the vector-
181 overexpression control. Viral replication was increased upon overexpression of WT HuR but
182 not S318A HuR, which did not relocalize to the cytoplasm and was rescued by
183 overexpression of S318D HuR (Fig 3G, H). This finding confirmed the importance of S318
184 phosphorylation in HuR localization and hence, HCV replication.

185 **PKC-δ activity is required for HCV-mediated cytoplasmic export of HuR**

186 Once the involvement of S318 phosphorylation in guiding HuR localization was ascertained,
187 we determined the role of the kinase responsible for this modification. An earlier study
188 suggested that PKC-δ participated in the phosphorylation of S318 on HuR and its
189 nucleocytoplasmic shuttling (Grammatikakis et al., 2017). Therefore, the involvement of
190 PKC-δ in regulating HuR localization upon HCV infection was investigated (Fig 4A). The

191 levels of total and phosphorylated PKC-δ at different time points after HCV infection were
192 analyzed. An increase in p-PKC-δ/total PKC-δ after 48h of HCV-RNA transfection was
193 observed, suggesting the activation of PKC-δ upon HCV infection (Fig 4B). To visualize the
194 interaction between HuR and PKC-δ in cells, immunoprecipitation of HuR was performed in
195 mock (control) and HCV-infected cells, and the presence of PKC-δ in the pull-down fraction
196 confirmed their physical interaction (Fig 4C). The increase in HuR associated with PKC-δ
197 indicated a stronger interaction in cells upon HCV infection. The association was further
198 strengthened by reverse pull-down, wherein immunoprecipitation of PKC-δ was performed
199 and increased HuR association was observed upon HCV infection (Fig 4D). To correlate this
200 finding with HuR localization, an inhibitor of PKC-δ (rottlerin) was used. The effect of PKC-
201 δ inhibition on HCV-induced HuR relocalization was assessed. Huh7.5 cells were transfected
202 with HCV-JFH1 RNA and 3 μM rottlerin was added to the medium after 6 h of transfection
203 (Fig 4E). The cells were incubated with the inhibitor for 48h, after which HuR localization
204 was visualized by confocal microscopy.

205 In the absence of the inhibitor, HuR relocated from the nucleus to the cytoplasm upon HCV
206 infection (Fig 4F, G). The presence of the inhibitor did not alter the localization of HuR in
207 control cells, but it prevented its relocalization to the cytoplasm upon HCV infection. These
208 results confirmed the involvement of PKC-δ in altering the localization of HuR upon HCV
209 infection.

210 **PKC-δ regulates the HCV life cycle through HuR**

211 Given that HuR is involved in viral RNA replication, we investigated the effect of rottlerin on
212 HCV-RNA levels. Huh7.5 cells were transfected with HCV-JFH1 RNA and 3 μM rottlerin
213 was added to the medium for 24h (Fig 5A). After 24h, the abundance of viral RNA in the
214 cells was quantified by real-time PCR, which showed that addition of rottlerin decreased

215 HCV-RNA levels by > 90% (Fig 5B). Similarly, confocal microscopy indicated that the
216 percentage of infected cells dropped from ~20% in untreated cells to <2% in rottlerin-treated
217 cells (Fig 5C, D). In all assays, the PKA inhibitor KT5720 was used as a negative control,
218 which did not show any effect on HuR localization upon HCV infection.

219 The expression of PKC-δ in healthy and hepatocellular carcinoma patients in The Cancer
220 Genome Atlas (TCGA) database was analyzed. Increased PKC-δ expression in virus-induced
221 hepatocellular carcinoma patients suggested its involvement in disease progression (Fig 5E),
222 and survival probability was inversely proportional to PKC-δ expression levels (Fig 5F). This
223 result suggested that patients with elevated PKC-δ would have more and early relocalisation
224 of HuR upon HCV infection, which would lead to enhanced viral replication and, hence,
225 increased likelihood of severe disease progression.

226 **HCV non-structural proteins are involved in HuR relocalization**

227 Activation of PKC-δ and relocalization of HuR seemed to be a viral strategy for its efficient
228 replication. Therefore, candidate viral protein(s) involved in PKC-δ activation were
229 investigated. Over-expression of either the structural protein, Core or all the non-structural
230 proteins together through pSGR-Luc construct was performed in Huh7.5 cells and
231 localization of HuR was assessed after 48h of overexpression. Viral non-structural proteins
232 were found to be sufficient to cause the relocalization of HuR (Fig 6A, B). Among non-
233 structural proteins, NS3 is a major pathogenic protein that interacts with multiple host
234 proteins and kinases (Borowski, Oehlmann et al., 1997, Borowski, zur Wiesch et al., 1999,
235 Lu, Zhang et al., 2015, Otsuka, Kato et al., 2005). To assess the physical interaction between
236 NS3 and PKC-δ, PKC-δ was modeled with the I-TASSER tool and docked with the available
237 NS3 structure using Pydockweb. Based on the docked structure with the lowest energy (Fig
238 6C), NS3 was found to interact with PKC-δ near its activation loop (highlighted in magenta).

239 The distance between NS3 and the T505 activation phosphorylation site of PKC-δ was ~11
240 Å, indicating possible regulation of phosphorylation and thereby PKC-δ activation. Similar
241 docking with other non-structural proteins NS5A and NS5B did not show close association
242 around T505 of PKC-δ (Fig 6D,E).

243 **AMPK is involved in cytoplasmic retention of HuR upon HCV infection**

244 Viral infection leads to HuR relocalization to the cytoplasm; however, at the same time, it is
245 essential for the virus that HuR is prevented from reentry in the nucleus. The nuclear
246 localization signal for HuR is not very well characterized. AMPK has been shown to
247 phosphorylate and acetylate importin-α1, which carries newly synthesized HuR to the
248 nucleus. Here, we assessed whether this mechanism was disrupted during HCV infection,
249 thus allowing HuR to be retained in the cytoplasm. Huh7.5 cells were treated with an AMPK
250 inhibitor (Compound C) or an AMPK activator (A769662) following HCV-RNA
251 transfection. HuR localization was assessed by confocal microscopy 48h after drug treatment.
252 Inhibition of AMPK activity did not alter HuR localization, whereas activation of AMPK led
253 to HuR transport back to the nucleus, even upon HCV infection (Fig 7A, B). To correlate
254 AMPK activity with hepatocellular carcinoma progression, TCGA database AMPK levels
255 were analyzed. A decrease in total AMPKα1 levels was observed upon virus-induced tumor
256 progression (Fig 7C). No significant correlation was observed between survival probability
257 and AMPK-α1 levels (Fig 7D). The viral non-structural protein NS5A inhibits AMPK
258 activity (Mankouri, Tedbury et al., 2010, Meng, Liu et al., 2019), and we showed here that
259 this inhibition was responsible for the cytoplasmic retention of HuR.

260 Our results uncovered the participation of multiple viral proteins in achieving increased
261 cytoplasmic abundance of HuR. We describe the underlying mechanism wherein viral RNA
262 translates upon entry into the cell, producing viral proteins. Viral NS3 protein activates PKC-

263 δ, which phosphorylates HuR on S318, leading to its relocalization to the cytoplasm, where it
264 is available for the replication of cytoplasmic viral RNA. At the same time, viral NS5A
265 protein inhibits AMPK, which retains relocalized and newly synthesized HuR in the
266 cytoplasm (Fig 8). The proposed mechanism depicts a coordinated effort to regulate a host
267 RNA binding protein, so it can be exploited to guide the viral life cycle.

268 **Discussion**

269 HCV is a hepatotropic virus that can cause chronic infection, leading to hepatocellular
270 carcinoma. Host factors play an essential role in regulating the virus life cycle and cellular
271 pathogenesis. HCV is a positive-strand RNA virus, whose RNA is replicated and translated in
272 the cytoplasm. RNA binding proteins (RBPs) such as HuR bind to viral RNA and regulate
273 these processes.

274 HCV is a completely cytoplasmic virus with no nuclear history of viral RNA. Therefore, it
275 mediates the relocalization of RBPs to the cytoplasm to enable RNA binding. We show that
276 phosphorylation of the S318 residue on HuR is essential for this relocalization. This site lies
277 in RRM3 of HuR, which is critical for its binding to HCV-RNA. Indeed, we demonstrate that
278 phosphorylation of S318 promotes the binding of HuR to HCV-RNA. Altered S318
279 phosphorylation levels have been detected in various pathologies such as colon cancer
280 (Doller et al., 2011), suggesting that the same could happen in hepatocellular carcinoma. We
281 report that S318 phosphorylation is mediated by PKC-δ. Inhibition of PKC-δ by lenvatinib
282 has recently been associated with decreased tumorigenicity in Huh7 and Hep3B
283 hepatocellular carcinoma cells (Wu, Hsu et al., 2022). One of the underlying mechanisms
284 behind the pro-proliferative effect of PKC-δ could be its regulation of HuR localization in
285 cells, which directly influences the cellular transcripts involved in tumorigenicity. These

286 reports and the evidence presented herein point to the key role of S318 phosphorylation in the
287 transport of HuR to the cytoplasm and in HCV infection.

288 HuR is not known to be mutated in many cancers. However, its localization and binding to
289 different RNA transcripts affect cancer progression (Wang, Guo et al., 2013). Reduced
290 AMPK activity, which leads to cytoplasmic localization of HuR, is known to stabilize
291 oncogenic molecules that promote progression of the proliferative phenotype. Here, we show
292 that this mechanism is activated also by HCV, pointing to the significant role of HuR
293 cytoplasmic localization in the progression of HCV-mediated hepatocellular carcinoma. HuR
294 targets include invasive and metastatic RNAs (e.g., MMP-9, MTA1, and uPA), angiogenic
295 RNAs (e.g., VEGF-1 and HIF-1), and cell proliferative RNAs (e.g., EGF, cyclin A, cyclin
296 B1, cyclin E, and cyclin D1), through which it can influence hepatocellular carcinoma
297 progression (Chen, Dai et al., 2020, Papatheofani, Levidou et al., 2021). By stabilizing these
298 target RNAs and increasing their protein products, HuR promotes the transformation from
299 non-cancerous to cancerous cells. Hence, HuR has been proposed as a potential target for
300 cancer treatment (Wu, Tong et al., 2019).

301 AMPK regulates the availability of HuR to the above RNAs in the cytoplasm. AMPK levels
302 and activity are reduced in patients with hepatocellular carcinoma, and low p-AMPK levels
303 correlate with higher tumor occurrence (Jiang, Tan et al., 2019, Yang, Liu et al., 2018).
304 Regulation of pathogenic RNAs by cytoplasmic HuR may be one of the mechanisms
305 underlying this correlation. AMPK is a double-edged sword, which influences cell
306 proliferation in either way. A recent report has shown that the effect of AMPK on cell
307 proliferation is a function of nutrient abundance. In cancer cells subjected to chronic nutrient
308 deprivation, AMPK inactivation limits cell proliferation (Sadria, Seo et al., 2022). This
309 limitation could be explained by direct activation of mTORC1 and mTORC2. Another
310 possibility is the cytoplasmic retention of HuR, which is known to stabilize and enhance the

311 translation of rictor, thereby activating mTORC2 (Holmes, Benavides-Serrato et al., 2018).
312 This could be one of the mechanisms of regulation of viral replication in cells and
313 hepatocellular carcinoma progression.

314 PKC-δ and AMPK are important cellular kinases that direct cell fate under various
315 conditions. HCV exploits these kinases to regulate replication and pathogenesis through HuR.
316 Preventing the cytoplasmic relocalization of HuR by either PKC-δ inhibition or AMPK
317 activation could offer a novel therapeutic intervention against hepatocellular carcinoma
318 progression.

319 **Materials and methods**

320 ***Plasmids and constructs:***

321 *pJFH1*: Plasmid encoding all HCV proteins. The plasmid was linearized using XbaI to
322 synthesise JFH1 RNA (Obtained from Apath,LLC).

323 *pSGR-JFH1/Luc*: Bicistronic plasmid where the luciferase expression is driven by HCV-
324 IRES while HCV non-structural proteins are expressed by EMCV IRES. The plasmid was
325 linearised by XbaI to synthesise SGR-JFH1/Luc RNA (A kind gift from Dr. Ralf
326 Bartenschlager, Heidelberg University).

327 *pcDNA3.1-myc-HuR*: The sequence coding for HuR cloned between EcoRI and XhoI sites of
328 pcDNA3.1-myc vector.

329 *HuR mutants:* HuR mutants were generated in the pcDNA3.1-myc-HuR background by site
330 directed mutagenesis and the mutations were confirmed by sequencing

331 ***Cell Lines and Transfections***

332 Huh7.5 cells were maintained in Dulbecco's Modified Eagle Medium DMEM (Sigma) with
333 10 % Fetal Bovine Serum. Lipofectamine 2000 (Invitrogen) was used for JFH1 RNA
334 transfections and TurboFect (Thermo Scientific) was used for DNA transfections according

335 to manufacturer's protocol. For generation of the infectious virus, HCV-JFH1 RNA was *in*
336 *vitro* transcribed and transfected into Huh7.5 cells. Supernatant from the transfected cells was
337 concentrated and used for viral infection. Uninfected Huh7.5 cells were used as a mock
338 control.

339 ***2D-gel electrophoresis:***

340 The protein lysates for Mock and HCV transfected samples were precipitated using 10 %
341 TCA and pellets washed with acetone. The protein pellets were resuspended in sample
342 rehydration buffer (8 M urea, 2 % [wt/vol] 3-[(3-cholamidopropyl)-dimethylammonio]-1-
343 propanesulfonate [CHAPS], 15 mM dithiothreitol [DTT], and 0.5 % [vol/vol] IPG buffer [pH
344 3 to 10]). Isoelectric focusing was performed using immobilized pH gradient (IPG) strips
345 (Bio-Rad). IPG strips with a pH range from 3 to 10 were used. For the first dimension, 500
346 µg of protein samples in 150 µl of rehydration solution was used to rehydrate the IPG strip (7
347 cm [length]; pH 3 to 10). The IPG strips were passively rehydrated overnight, and then the
348 proteins were focused for 10,000V. h at 20 °C under mineral oil. After focusing, the strips
349 were incubated for 10 min in 2 ml of equilibrium buffer I (6 M urea, 30 % [wt/vol] glycerol,
350 2 % [wt/vol] sodium dodecyl sulfate [SDS], and 1 % [wt/vol] DTT in 50 mM Tris-HCl buffer
351 [pH 8.8]), followed by equilibrium buffer II (6 M urea, 30 % [wt/vol] glycerol, 2 % [wt/vol]
352 SDS, and 4 % [wt/vol] iodoacetamide in 375 mM Tris-HCl buffer [pH8.8]). After the
353 equilibration steps, the strips were transferred to a 12 % SDS-polyacrylamide gel
354 electrophoresis (PAGE) gel for the second dimension. Protein spots were visualized by silver
355 staining.

356 ***Immunofluorescence staining***

357 For immunofluorescence staining, ~$0.2*10^6$ Huh7.5 cells were seeded on coverslips in a 12-
358 well plate for 14 h followed by transfection of HCV-JFH1 RNA (1µg). After desired time of

359 infection/ RNA transfection, cells were washed twice with 1X PBS and fixed using 4 %
360 formaldehyde at room temperature for 20 min. After permeabilization by 0.1 % Triton X-100
361 for 2 min at room temperature, cells were incubated with 3 % BSA at 37 °C for 1 h followed
362 by incubation with the indicated antibody for 2 h at 4 °C and then detected by Alexa-633-
363 conjugated anti-mouse or Alexa-488 conjugated anti-rabbit secondary antibody for 30 min
364 (Invitrogen). Images were taken using Zeiss microscope and image analysis was done using
365 the Zeiss LSM or ZEN software tools.

366 ***Western-blot analysis:***

367 Protein concentrations of the extracts were assayed by Bradford reagent (Bio-Rad) and equal
368 amounts of cell extracts were separated by SDS-12 % PAGE and transferred onto a
369 nitrocellulose membrane (Sigma). Samples were then analyzed by western blot using the
370 desired antibodies, anti-HCV core antibody (ab2740, Abcam), anti-HuR antibody (3A2,
371 Santa Cruz and 07-1735, Merck Millipore), anti-pan-p-Ser/Thr antibody (AP0893, Abclonal),
372 anti-pan-p-Tyr antibody (AP0905, Abclonal), anti-PKC-δ antibody (A7778, Abclonal), anti-
373 p-PKC-δ-T505 (AP0776) followed by the respective secondary antibodies (horseradish
374 peroxidase-conjugated anti-mouse or anti-rabbit IgG; Sigma). Mouse-monoclonal anti-β-
375 actin- peroxidase antibody (A3854, Sigma) was used as a control for equal loading of total
376 cell extracts. Antibody complexes were detected using the ImmobilonTM Western systems
377 (Millipore).

378 ***Immunoprecipitation:***

379 Huh7.5 cells were scraped in polysome lysis buffer (100 mM KCl, 5 mM $MgCl_2$, 10 mM
380 HEPES pH 7.0, 0.5 % NP-40, 1 mM DTT, 100 U/ml RNasin) and kept on cyclomixer for 1 h,
381 followed by spinning at 16000×g for 15 min at 4 °C. The supernatant obtained was
382 precleared with Protein G Sepharose beads for 1 h at 4 °C. The samples were spun at 1000×g
383 for 2 min to pellet the beads, and the supernatant was removed. Protein G Sepharose beads

384 were incubated with 1 ug of respective antibody overnight at 4 °C in a total volume of 200 µl
385 of polysome lysis buffer and added to the precleared lysates followed by incubation for 3 h
386 with continuous mixing on a rotator device at 4°C. The beads were washed three times with
387 polysome lysis buffer. SDS sample buffer was then added to the beads and boiled to release
388 the immunoprecipitated protein, and the supernatant was electrophoresed on a SDS-12 %
389 PAGE.

390 ***Surface Plasmon Resonance:***

391 Surface plasmon resonance spectroscopy was performed using a BIAcore3000 optical
392 biosensor (GE Healthcare Lifescience) to study the binding kinetics of HuR with SARS
393 CoV2 5'UTR RNA. Biotin-labelled HCV 3'UTR RNA was immobilized on streptavidin-
394 coated sensor chips (GE Healthcare Lifescience) to a final concentration of 300 Resonance
395 Units (RU)/flow cell. RNA–protein interactions were carried out in a continuous flow of Tris
396 buffer (25 mM Tris (pH 7.5), 100 mM KCl, 7 mM β-mercaptoethanol, and 10% glycerol) at
397 25 °C at a flow rate of 10 µl/min. Increasing concentrations of HuR protein loaded on the
398 biosensor chip for 100 s (characterized as the association phase), followed by a dissociation
399 phase of 300 s with buffer alone. For normalising background non-specific interaction, a
400 blank surface without any RNA was used for simultaneous injections of the sample during
401 the experiment. BIAevaluation software (version 3.0) was used to determine the on rate, *k*on
402 (M^{-1} s^{-1}), and off rate, *k*off (s^{-1}), using a 1:1 Langmuir binding model. The binding affinity,
403 *Kd* was determined using the following equation: *Kd* =*k*off/*k*on.

404 ***Molecular docking of HCV-NS3 and PKC-δ:***

405 For molecular docking of PKC-δ with HCV-NS3, PKC-δ sequence was taken from NCBI and
406 structure was predicted using I-TASSER server. For HCV-NS3, structure with PDB ID:
407 5WDX was used. pyDOCK webtool was used for blind docking of the two molecules. The
408 result file with lowest energy has been demonstrated.

409 ***Immunoprecipitation of HuR followed by Mass spectrometry:***

410 Huh7.5 cells were transfected with HCV-JFH1 RNA and harvested after 48h of transfection.
411 Total proteins were extracted in IP lysis buffer (Pierce, Thermo Scientific) containing 1×
412 halt-protease and phosphatase inhibitor cocktail (Thermo Fisher Scientific, USA) with
413 intermediate vortexing followed by mild sonication. The lysate was centrifuged at 14,000 × g
414 for 30 min at 4 °C. The supernatant was quantified by the BCA method (Thermo Fisher
415 Scientific, USA). An equivalent amount (4 mg) of proteins from each condition was
416 incubated with 3µg of anti-HuR antibody for overnight at 4 °C. The immunocomplex was
417 captured by using protein G Sepharose 4 fast flow beads (17-0618-01/ GE Healthcare). The
418 immunoprecipitated complex was washed two times with IP lysis buffer and one time with
419 mili-Q. Bound protein complexes were eluted in 50 µl SDS-PAGE 2X Laemmli sample
420 buffer. The samples were resolved on 12% SDS–PAGE and stained with Coomassie stain
421 (0.1% w/v). The gel was subjected to further in-gel mass spectrometry analysis.

422 Gel slices corresponding to each lane were excised in individual eppendorf and destained
423 using wash buffer (50 mM ammonium bicarbonate (ABC) and 50% ACN). Slices were
424 hydrated with 10 mM DTT (56°C, 30 min), alkylated using 50 mM IAA (30 min, RT, dark),
425 and further dehydrated using 100% ACN before digestion. The available proteins in-gel
426 pieces were digested with MS grade trypsin (Pierce™ Trypsin Protease MS grade, cat no.
427 1862743, USA) and incubated at 37 °C for 18 h. Digested peptides were extracted by adding
428 60% ACN with 0.1% FA and 100% ACN with 0.1% FA, followed by ultra-sonication. The
429 digested peptides were collected, vacuum dried, and reconstituted in 40 µl of solvent A (2%
430 (v/v) ACN, 0.1% (v/v) FA in water) and subjected to LC−MS/MS experiments using Sciex
431 5600^{+} Triple-TOF mass spectrometer coupled with ChromXP reversed-phase 3 µm C18-CL
432 trap column (350 µm × 0.5 mm, 120 Å, Eksigent, AB Sciex) and nanoViper C18 separation
433 column (75 µm × 250 mm, 3 µm, 100 Å; Acclaim Pep Map, Thermo Scientific, USA) in

434 Eksigent nanoLC (Ultra 2D plus) system. The binary mobile solvent system was consisted
435 with solvent A (2% (v/v) ACN, 0.1% (v/v) FA in water) and solvent B (98% (v/v) ACN,
436 0.1% (v/v) FA). The peptides were analysed with 300 nl/min flow rate in a 60 min gradient
437 with a total run time of 75 minutes. The acquisition was executed with conventional data-
438 dependent IDA mode. Each cycle consisted of 250 and 100 ms acquisition time for MS1 (m/z
439 350−1250 Da) and MS/MS (100–1500 m/z) scans respectively with a total cycle time of 2.8
440 s. Each fraction was run in duplicate.

441 ***Phospho-peptide and phospho-site identification***

442 All raw files (.wiff) were processed to ProteinPilot software (version 4.5, SCIEX) using the
443 Paragon algorithm (version 4. 5. 0. 0,1654). The phospho-peptides along with phospho-sites
444 were identified against the complete sequence of Hepatitis C virus JFH-1 polyprotein. The
445 identification settings were used as follows: (a) trypsin for proteolytic cleavage (b) Iodoacetic
446 acid used for Cys alkylation and (c) phosphorylation emphasis used as a special factor.
447 Peptides and proteins were validated at <1% false discovery rate (FDR) and with unused
448 ProtScore > 0.05.

449 **Acknowledgments**

450 SD acknowledges the J.C. Bose Fellowship from the Department of Science and Technology
451 (DST), Govt. of India, for research support. This study was also supported by the DBT-IISc
452 partnership program, DST Fund for Improvement of Science and Technology Infrastructure
453 (DST- FIST) level II infrastructure, and the University Grants Commission Centre of
454 Advanced Studies. We also acknowledge the funding through Indo-Swiss Joint Research
455 Program (ISJRP) from Department of Biotechnology. HR is supported by the research
456 fellowship from the Council of Scientific and Industrial Research (CSIR-SPM). We
457 recognize the divisional SPR facility at the Biological Science division at IISc.

458 **Author contributions**

459 HR and SD: Conceptualisation, design, analysis and interpretation of experiments, and
460 manuscript writing. HR, BG, SS, SM and TKM: Performing the experiments.

461 **Disclosure statement**

462 The authors state they have no competing interests or disclosures.

463 **Figure legends**

464 **Figure 1. HuR gets phosphorylated upon HCV infection.**

465 **(A)** Huh7.5 cells were transfected with HCV-JFH1 RNA. Mock and transfected cells were
466 harvested after 48h and cell lysates were precipitated using TCA precipitation. The
467 precipitated proteins were run in 2 dimensions as described in the methods, followed by
468 Western blotting of the gel. Western blotting was done with anti-HuR and anti-Actin
469 antibodies. Appropriate HRP-conjugate secondary antibodies were used.

470 **(B)** HCV infection was detected by western blotting using Anti-HCV core antibody for same
471 lysates run on 12% SDS-PAGE.

472 **(C)** Schematic for experimental protocol followed.

473 **(D)** Huh 7.5 cells were transfected with Myc-tagged overexpression construct of WT HuR,
474 S318A HuR mutant, S242A HuR mutant, Y200F HuR mutant, T118A HuR mutant and
475 S221A HuR mutant and mock transfected. Cells were processed for immunofluorescence
476 staining using Alexa Fluor conjugated secondary antibody against Myc (Green) and viral
477 protein Core (Red). The nucleus was stained with DAPI (Blue). Scale bar represents 10 µm.

478 **(E)** Nuclear and cytoplasmic ratio was quantified for images in (D) using Zen 2.3 lite
479 software.

480 **(F)** Images of HCV transfected cells following the schematic in (C).

481 **(G)** Nuclear and cytoplasmic ratio was quantified for images in (F) using Zen 2.3 lite
482 software. n=10.

483 Student t-test was performed for statistical analysis. *= $p<0.05$, **= $p<0.01$, ***=$p<0.001$.

484 **Figure 2. Differential phosphorylation on HuR upon HCV infection.**

485 **(A, B)** Huh7.5 cells were mock transfected or transfected with HCV-JFH1 RNA and after
486 48h, immunoprecipitation was performed using either anti-p-Ser/Thr antibody (A) or anti-p-
487 Tyr antibody (B). Associated HuR was detected by western blot. Western blot for Core was
488 done for confirmation of HCV infection and β-actin was used as loading control.

489 **(C)** Identification of phosphorylation sites on HuR. Immunoprecipitation of HuR was
490 performed from mock or HCV-JFH1 RNA transfected cells and the phosphorylation sites
491 detected using mass-spectrometry.

492 **(D)** HCV infection was confirmed by western blotting for Core using anti-core antibody.

493 **(E)** The phosphorylation sites obtained in mass-spectrometry data were mapped on HuR
494 schematic diagram.

495 **(F-H)** Percentage of phosphorylated S318 (F), S202 (G), S135 (H) sites were calculated as
496 the ratio of peptides containing phosphorylation to the total number of peptides containing
497 respective site. Each dot pair represents a separate set of experiment.

498 **Figure 3. S318 site phosphorylation influences HCV-RNA replication.**

499 **(A)** S318 site in HuR RRM3 in association with AU-rich RNA. The red balls indicate S318
500 site, directly involved in interaction with associated RNA.

501 **(B-D)** Sensorgrams for interaction of (B) WT, (C) S318D HuR and (D) S318A HuR with
502 HCV 3'UTR at indicated concentrations. The y-axis represents the change in Response Units
503 in Association and dissociation phases and x-axis represents time.

504 **(E)** Table for the average Kd value obtained for HuR binding to HCV 3'UTR.

505 **(F)** Schematic for the workflow.

506 **(G)** Following the workflow in (F), total cellular RNA was isolated, and HCV negative strand
507 RNA detected by real time PCR (n=3).

508 **(H)** Western blotting for HuR was performed following the workflow in (F).

509 Student t-test was performed for statistical analysis. *= $p<0.05$, **= $p<0.01$, ***=$p<0.001$.

510 **Figure 4. Involvement of PKC-δ in HuR localisation.**

511 **(A)** Table for kinase known for S318 site of HuR.

512 **(B)** Huh7.5 cells were transfected with HCV-JFH1 RNA and cells harvested at indicated
513 time-points. Western blotting was done with anti-PKCδ, anti-p-PKCδ, anti-Core and anti-
514 actin antibodies. Appropriate HRP-conjugate secondary antibodies were used.

515 **(C)** Immuno-pulldown of HuR was performed from Huh7.5 cells, post 72h of HCV infection
516 and associated PKC-δ was checked by western blotting with specific antibody. The values at
517 bottom represent ratio of densitometry values of PKC-δ in the IP fraction to that of HuR in IP
518 fraction.

519 **(D)** Immuno-pulldown of PKC-δ was performed from Huh7.5 cells, post 72h of HCV
520 infection and associated HuR was checked by western blot using HuR-specific antibody. The
521 values at bottom represent ratio of densitometry values of HuR in the IP fraction to that of
522 PKC-δ in IP fraction.

523 **(E, F)** Huh7.5 cells were treated with infectious HCV-JFH1 virus in the presence of 3μM of
524 Rottlerin and immunofluorescence staining was carried out at 24h post infection using Alexa
525 Fluor conjugated secondary antibodies against HCV-NS3 (Red) or HuR (Green). The nucleus
526 was counterstained with DAPI. Scale bar represents 10 μm.

527 **(G)** Nuclear and cytoplasmic ratio was quantified for images in (F) using Zen 2.3 lite
528 software. n=30. Student t-test was performed for statistical analysis. *= $p<0.05$, **= $p<0.01$,
529 ***=$p<0.001$.

530 **Figure 5. Role of PKC-δ. In HCV life cycle.**

531 **(A)** Workflow of the experiment.

532 **(B)** According to the workflow, cells were harvested after 24h of addition of inhibitors. Total
533 RNA was isolated from the cells and HCV negative strand RNA was detected using RT-
534 qPCR. Fold change in RNA levels was calculated as compared to RNA levels in cells with no
535 inhibitor treatment. (n=3)

536 **(C)** Huh7.5 cells were transfected with HCV-JFH1 RNA in the presence of 3μM of Rottlerin
537 or 10μ*M* KT5720 and immunofluorescence staining was carried out at 24h post infection
538 using Alexa Fluor conjugated secondary antibodies against HCV-NS3 (Red). The nucleus
539 was counterstained with DAPI. Scale bar represents 100μm.

540 **(D)** Quantification of the confocal images in panel C. (n=3)

541 **(E)** Expression level of PKC-δ (PRKCD gene) in healthy tissue and Virus induced primary
542 HCC tissue samples from TCGA database.

543 **(F)** Kaplan Meier plot for survival probability for Virus induced primary HCC patients with
544 varying level of expression of PKC-δ. Data taken from TCGA database.

545 Student t-test was performed for statistical analysis. *= $p<0.05$, **= $p<0.01$, ***=$p<0.001$.

546 **Figure 6. Viral protein involved in relocalisation of HuR.**

547 **(A)** Huh7.5 cells were transfected with plasmid expressing HCV protein as indicated.
548 Immunofluorescence staining was carried out at 24h post transfection using Alexa Fluor
549 conjugated secondary antibodies against HuR (Green) and indicated viral proteins (Red). The
550 nucleus was counterstained with DAPI. Scale bar represents 20µm.

551 **(B)** Nuclear and cytoplasmic ratio was quantified for images in (A) using Zen 2.3 lite
552 software. n=10.

553 **(C)** Molecular docking for NS3 and PKC-δ interaction. The structure of PKC-δ was modelled
554 using the software I-TASSER and docked with NS3 structure using Pydockweb. Cyan color
555 represents NS3, green color represents PKC-δ and magenta represents the activation loop in
556 PKC-δ.

557 **(D)** Molecular docking for NS5A and PKC-δ interaction. The structure of PKC-δ was
558 modelled using the software I-TASSER and docked with NS5A structure using Pydockweb.
559 Cyan color represents NS5A, green color represents PKC-δ and magenta represents the
560 activation loop in PKC-δ.

561 **(E)** Molecular docking for NS5B and PKC-δ interaction. The structure of PKC-δ was
562 modelled using the software I-TASSER and docked with NS5B structure using Pydockweb.
563 Cyan color represents NS5B, green color represents PKC-δ and magenta represents the
564 activation loop in PKC-δ.

565 Student t-test was performed for statistical analysis. *= $p<0.05$, **= $p<0.01$, ***=$p<0.001$.

566 **Figure 7. AMPK in relocalisation of HuR.**

567 **(A)** Huh7.5 cells were transfected with HCV-JFH1 RNA in the presence of 10µM of AMPK
568 inhibitor Compound C (CC) or 100mM A76 and immunofluorescence staining was carried

569 out after 48h using Alexa Fluor conjugated secondary antibodies against HCV-Core (Red)
570 and HuR (Green). The nucleus was counterstained with DAPI. Scale bar represents 20µm.

571 **(B)** Nuclear and cytoplasmic ratio was quantified for images in (A) using Zen 2.3 lite
572 software. n=30.

573 **(C)** Expression level of PRKAA2 (AMPKα2) in healthy tissue, HCC primary tumor samples
574 and Virus induced primary HCC tissue samples from TCGA database.

575 **(D)** Kaplan Meier plot for survival probability for Virus induced primary HCC patients with
576 varying level of expression of AMPKα2. Data taken from TCGA database.

577 Student t-test was performed for statistical analysis. *= $p<0.05$, **= $p<0.01$, ***=$p<0.001$.

578 **Figure 8. Proposed mechanism of HuR relocalisation upon HCV infection.** (0) Cellular
579 mechanism of HuR transport to nucleus. AMPK phosphorylates Importin-α1 which guides
580 HuR to the nucleus. (1) HCV entry in the cells followed by Viral RNA release in the cell
581 cytoplasm. (2) Viral RNA translates to produce structural and non-structural proteins. (3)
582 Non-structural protein 3, NS3, activates PKC-δ. (4) PKC-δ phosphorylates HuR on S318
583 residue, guiding its cytoplasmic export. (5) Non-structural protein 5A, NS5A, inhibits AMPK
584 to retain the cytoplasmically relocalised and new synthesised HuR in the cytoplasm. (6) The
585 cytoplasmically localised HuR assists in viral replication by binding to viral 3'UTR.

586 **References**

587 Abdelmohsen K, Pullmann R, Jr., Lal A, Kim HH, Galban S, Yang X, Blethrow JD, Walker M, Shubert J,
588 Gillespie DA, Furneaux H, Gorospe M (2007) Phosphorylation of HuR by Chk2 regulates SIRT1
589 expression. *Molecular cell* 25: 543-57

590 Bonamassa B, Ciccarese F, Antonio VD, Contarini A, Palù G, Alvisi G (2015) Hepatitis C virus and host
591 cell nuclear transport machinery: a clandestine affair. 6

592 Borowski P, Oehlmann K, Heiland M, Laufs RJJov (1997) Nonstructural protein 3 of hepatitis C virus
593 blocks the distribution of the free catalytic subunit of cyclic AMP-dependent protein kinase. 71:
594 2838-2843

595 Borowski P, zur Wiesch JS, Resch K, Feucht H, Laufs R, Schmitz HJJoBC (1999) Protein kinase C
596 recognizes the protein kinase A-binding motif of nonstructural protein 3 of hepatitis C virus. 274:
597 30722-30728

598 Chen T, Dai X, Dai J, Ding C, Zhang Z, Lin Z, Hu J, Lu M, Wang Z, Qi Y, Zhang L, Pan R, Zhao Z, Lu L, Liao
599 W, Lu X (2020) AFP promotes HCC progression by suppressing the HuR-mediated Fas/FADD
600 apoptotic pathway. *Cell Death & Disease* 11: 822

601 Chu PC, Chuang HC, Kulp SK, Chen CS (2012) The mRNA-stabilizing factor HuR protein is targeted by
602 β-TrCP protein for degradation in response to glycolysis inhibition. *The Journal of biological*
603 *chemistry* 287: 43639-50

604 de Sousa GF, Lima Mde A, Custodio DF, Freitas VM, Monteiro G (2015) Chemogenomic Study of
605 Carboplatin in Saccharomyces cerevisiae: Inhibition of the NEDDylation Process Overcomes Cellular
606 Resistance Mediated by HuR and Cullin Proteins. *PLoS One* 10: e0145377

607 Dentzer TG, Lorenz IC, Evans MJ, Rice CM (2009) Determinants of the hepatitis C virus nonstructural
608 protein 2 protease domain required for production of infectious virus. *Journal of Virology* 83: 12702-
609 12713

610 Doller A, Akool el S, Huwiler A, Müller R, Radeke HH, Pfeilschifter J, Eberhardt W (2008)
611 Posttranslational modification of the AU-rich element binding protein HuR by protein kinase Cdelta
612 elicits angiotensin II-induced stabilization and nuclear export of cyclooxygenase 2 mRNA. *Molecular*
613 *and cellular biology* 28: 2608-25

614 Doller A, Huwiler A, Müller R, Radeke HH, Pfeilschifter J, Eberhardt W (2007) Protein kinase C alpha-
615 dependent phosphorylation of the mRNA-stabilizing factor HuR: implications for posttranscriptional
616 regulation of cyclooxygenase-2. *Molecular biology of the cell* 18: 2137-48

617 Doller A, Schlepckow K, Schwalbe H, Pfeilschifter J, Eberhardt W (2010) Tandem phosphorylation of
618 serines 221 and 318 by protein kinase Cdelta coordinates mRNA binding and nucleocytoplasmic
619 shuttling of HuR. *Molecular and cellular biology* 30: 1397-410

620 Doller A, Winkler C, Azrilian I, Schulz S, Hartmann S, Pfeilschifter J, Eberhardt W (2011) High-
621 constitutive HuR phosphorylation at Ser 318 by PKC{delta} propagates tumor relevant functions in
622 colon carcinoma cells. *Carcinogenesis* 32: 676-85

623 Fan XC, Steitz JA (1998) HNS, a nuclear-cytoplasmic shuttling sequence in HuR. 95: 15293-15298

624 Fialcowitz-White EJ, Brewer BY, Ballin JD, Willis CD, Toth EA, Wilson GM (2007) Specific Protein
625 Domains Mediate Cooperative Assembly of HuR Oligomers on AU-rich mRNA-destabilizing
626 Sequences*. *Journal of Biological Chemistry* 282: 20948-20959

627 Filippova N, Yang X, King P, Nabors LB (2012) Phosphoregulation of the RNA-binding protein Hu
628 antigen R (HuR) by Cdk5 affects centrosome function. *The Journal of biological chemistry* 287:
629 32277-87

630 Filippova N, Yang X, Nabors LB (2015) Growth factor dependent regulation of centrosome function
631 and genomic instability by HuR. *Biomolecules* 5: 263-81

632 Grammatikakis I, Abdelmohsen K, Gorospe M (2017) Posttranslational control of HuR function. *Wiley*
633 *Interdiscip Rev RNA* 8: 10.1002/wrna.1372

634 Gu M, Rice CM (2013) Structures of hepatitis C virus nonstructural proteins required for replicase
635 assembly and function. *Current opinion in virology* 3: 129-136

636 Holmes B, Benavides-Serrato A, Freeman RS, Landon KA, Bashir T, Nishimura RN, Gera J (2018)
637 mTORC2/AKT/HSF1/HuR constitute a feed-forward loop regulating Rictor expression and tumor
638 growth in glioblastoma. *Oncogene* 37: 732-743

639 Jiang X, Tan H-Y, Teng S, Chan Y-T, Wang D, Wang N (2019) The Role of AMP-Activated Protein
640 Kinase as a Potential Target of Treatment of Hepatocellular Carcinoma. *Cancers (Basel)* 11: 647

641 Jirasko V, Montserret R, Lee JY, Gouttenoire J, Moradpour D, Penin F, Bartenschlager R (2010)
642 Structural and Functional Studies of Nonstructural Protein 2 of the Hepatitis C Virus Reveal Its Key
643 Role as Organizer of Virion Assembly. *PLOS Pathogens* 6: e1001233

644 Kim HH, Abdelmohsen K, Lal A, Pullmann R, Jr., Yang X, Galban S, Srikantan S, Martindale JL,
645 Blethrow J, Shokat KM, Gorospe M (2008) Nuclear HuR accumulation through phosphorylation by
646 Cdk1. *Genes Dev* 22: 1804-1815

647 Kim HH, Yang X, Kuwano Y, Gorospe M (2008) Modification at HuR(S242) alters HuR localization and
648 proliferative influence. *Cell cycle (Georgetown, Tex)* 7: 3371-7

649 Kumar R, Mehta D, Mishra N, Nayak D, Sunil S (2020) Role of Host-Mediated Post-Translational
650 Modifications (PTMs) in RNA Virus Pathogenesis. *Int J Mol Sci* 22

651 Lafarga V, Cuadrado A, Lopez de Silanes I, Bengoechea R, Fernandez-Capetillo O, Nebreda AR (2009)
652 p38 Mitogen-activated protein kinase- and HuR-dependent stabilization of p21(Cip1) mRNA
653 mediates the G(1)/S checkpoint. *Molecular and cellular biology* 29: 4341-51

654 Liao WL, Wang WC, Chang WC, Tseng JT (2011) The RNA-binding protein HuR stabilizes cytosolic
655 phospholipase A2α mRNA under interleukin-1β treatment in non-small cell lung cancer A549 Cells.
656 *The Journal of biological chemistry* 286: 35499-35508

657 Lindenbach BD, Rice CM (2005) Unravelling hepatitis C virus replication from genome to function.
658 *Nature* 436: 933-938

659 Liwak-Muir U, Dobson CC, Naing T, Wylie Q, Chehade L, Baird SD, Chakraborty PK, Holcik M (2016)
660 ERK8 is a novel HuR kinase that regulates tumour suppressor PDCD4 through a miR-21 dependent
661 mechanism. *Oncotarget* 7: 1439-50

662 Lu L, Zhang Q, Wu K, Chen X, Zheng Y, Zhu C, Wu J (2015) Hepatitis C virus NS3 protein enhances
663 cancer cell invasion by activating matrix metalloproteinase-9 and cyclooxygenase-2 through
664 ERK/p38/NF-κB signal cascade. *Cancer letters* 356: 470-8

665 Ma W-J, Cheng S, Campbell C, Wright A, Furneaux H (1996) Cloning and Characterization of HuR, a
666 Ubiquitously Expressed Elav-like Protein (*). *Journal of Biological Chemistry* 271: 8144-8151

667 Mankouri J, Tedbury PR, Gretton S, Hughes ME, Griffin SDC, Dallas ML, Green KA, Hardie DG, Peers C,
668 Harris M (2010) Enhanced hepatitis C virus genome replication and lipid accumulation mediated by
669 inhibition of AMP-activated protein kinase. *Proc Natl Acad Sci U S A* 107: 11549-11554

670 Marceau CD, Puschnik AS, Majzoub K, Ooi YS, Brewer SM, Fuchs G, Swaminathan K, Mata MA, Elias
671 JE, Sarnow P, Carette JE (2016) Genetic dissection of Flaviviridae host factors through genome-scale
672 CRISPR screens. *Nature* 535: 159-163

673 Meng Z, Liu Q, Sun F, Qiao L (2019) Hepatitis C virus nonstructural protein 5A perturbs lipid
674 metabolism by modulating AMPK/SREBP-1c signaling. *Lipids in Health and Disease* 18: 191

675 Niepmann M, Gerresheim GK (2020) Hepatitis C Virus Translation Regulation. *International Journal*
676 *of Molecular Sciences* 21

677 Otsuka M, Kato N, Moriyama M, Taniguchi H, Wang Y, Dharel N, Kawabe T, Omata M (2005)
678 Interaction between the HCV NS3 protein and the host TBK1 protein leads to inhibition of cellular
679 antiviral responses. *Hepatology (Baltimore, Md)* 41: 1004-12

680 Papatheofani V, Levidou G, Sarantis P, Koustas E, Karamouzis MV, Pergaris A, Kouraklis G, Theocharis
681 S (2021) HuR Protein in Hepatocellular Carcinoma: Implications in Development, Prognosis and
682 Treatment. *Biomedicines* 9: 119

683 Ray U, Das S (2011) Interplay between NS3 protease and human La protein regulates translation-
684 replication switch of Hepatitis C virus. *Scientific Reports* 1: 1

685 Ripin N, Boudet J, Duszczyk MM, Hinniger A, Faller M, Krepl M, Gadi A, Schneider RJ, Šponer J,
686 Meisner-Kober NC, Allain FH-T (2019) Molecular basis for AU-rich element recognition and
687 dimerization by the HuR C-terminal RRM. 116: 2935-2944

688 Sadria M, Seo D, Layton AT (2022) The mixed blessing of AMPK signaling in Cancer treatments. *BMC*
689 *Cancer* 22: 105

690 Schultz CW, Preet R, Dhir T, Dixon DA, Brody JR (2020) Understanding and targeting the disease-
691 related RNA binding protein human antigen R (HuR). 11: e1581

692 Sharma G, Raheja H, Das S (2018) Hepatitis C virus: Enslavement of host factors. *IUBMB Life* 70: 41-
693 49

694 Shwetha S, Kumar A, Mullick R, Vasudevan D, Mukherjee N, Das S, Diamond MS (2015) HuR
695 Displaces Polypyrimidine Tract Binding Protein To Facilitate La Binding to the 3′
696 Untranslated Region and Enhances Hepatitis C Virus Replication. 89: 11356-11371

697 Srikantan S, Gorospe M (2012) HuR function in disease. *Front Biosci (Landmark Ed)* 17: 189-205

698 Vigouroux C, Casse JM, Battaglia-Hsu SF, Brochin L, Luc A, Paris C, Lacomme S, Gueant JL, Vignaud
699 JM, Gauchotte G (2015) Methyl(R217)HuR and MCM6 are inversely correlated and are prognostic
700 markers in non small cell lung carcinoma. *Lung cancer (Amsterdam, Netherlands)* 89: 189-96

701 Wang J, Guo Y, Chu H, Guan Y, Bi J, Wang B (2013) Multiple Functions of the RNA-Binding Protein
702 HuR in Cancer Progression, Treatment Responses and Prognosis. 14: 10015-10041

703 Wang W, Fan J, Yang X, Fürer-Galban S, Lopez de Silanes I, von Kobbe C, Guo J, Georas SN, Foufelle F,
704 Hardie DG, Carling D, Gorospe M (2002) AMP-activated kinase regulates cytoplasmic HuR. *Molecular*
705 *and cellular biology* 22: 3425-3436

706 Wang W, Yang X, Kawai T, de Silanes IL, Mazan-Mamczarz K, Chen P, Chook YM, Quensel C, Köhler
707 M, Gorospe M (2004) AMP-activated Protein Kinase-regulated Phosphorylation and Acetylation of
708 Importin α1: INVOLVEMENT IN THE NUCLEAR IMPORT OF RNA-BINDING PROTEIN HuR*. *Journal of*
709 *Biological Chemistry* 279: 48376-48388

710 Wu C-H, Hsu F-T, Chao T-L, Lee Y-H, Kuo Y-C (2022) Revealing the suppressive role of protein kinase C
711 delta and p38 mitogen-activated protein kinase (MAPK)/NF-κB axis associates with lenvatinib-
712 inhibited progression in hepatocellular carcinoma in vitro and in vivo. *Biomedicine &*
713 *Pharmacotherapy* 145: 112437

714 Wu M, Tong CWS, Yan W, To KKW, Cho WCS (2019) The RNA Binding Protein HuR: A Promising Drug
715 Target for Anticancer Therapy. *Current cancer drug targets* 19: 382-399

716 Yang X, Liu Y, Li M, Wu H, Wang Y, You Y, Li P, Ding X, Liu Ca, Gong J (2018) Predictive and preventive
717 significance of AMPK activation on hepatocarcinogenesis in patients with liver cirrhosis. *Cell death &*
718 *disease* 9: 264-264

719 Yoon JH, Abdelmohsen K, Srikantan S, Guo R, Yang X, Martindale JL, Gorospe M (2014) Tyrosine
720 phosphorylation of HuR by JAK3 triggers dissociation and degradation of HuR target mRNAs. *Nucleic*
721 *acids research* 42: 1196-208

722 Zhou HL, Geng C, Luo G, Lou H (2013) The p97-UBXD8 complex destabilizes mRNA by promoting
723 release of ubiquitinated HuR from mRNP. *Genes Dev* 27: 1046-58

724

Figure 1.

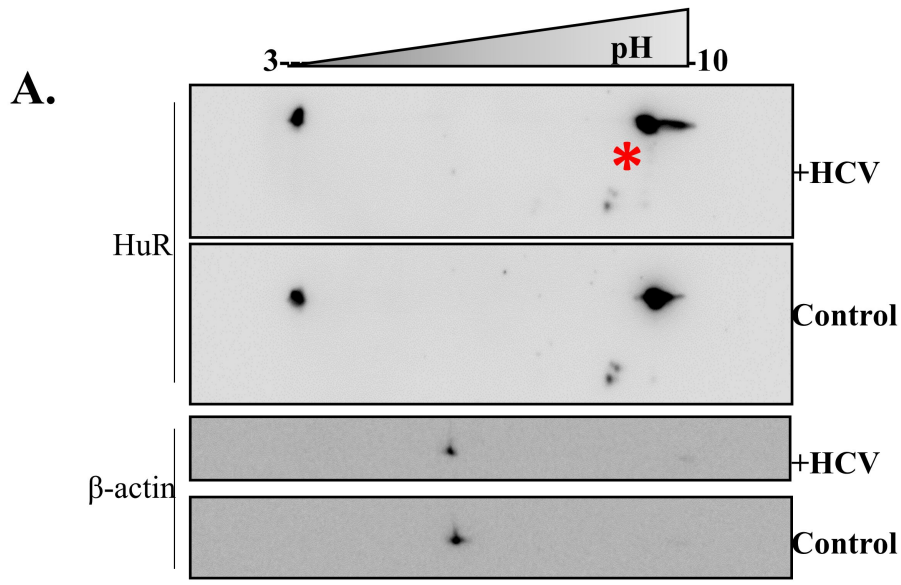
A.
3
pH
10
HuR
+HCV
Control
β-actin
+HCV
Control

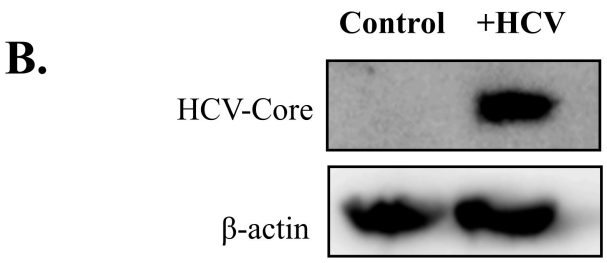
B.
Control
+HCV
HCV-Core
β-actin

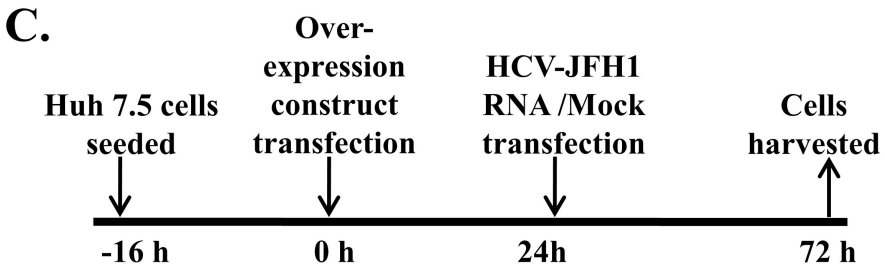
C.
Huh 7.5 cells seeded
Over-expression construct transfection
HCV-JFH1 RNA /Mock transfection
Cells harvested
-16 h
0 h
24h
72 h

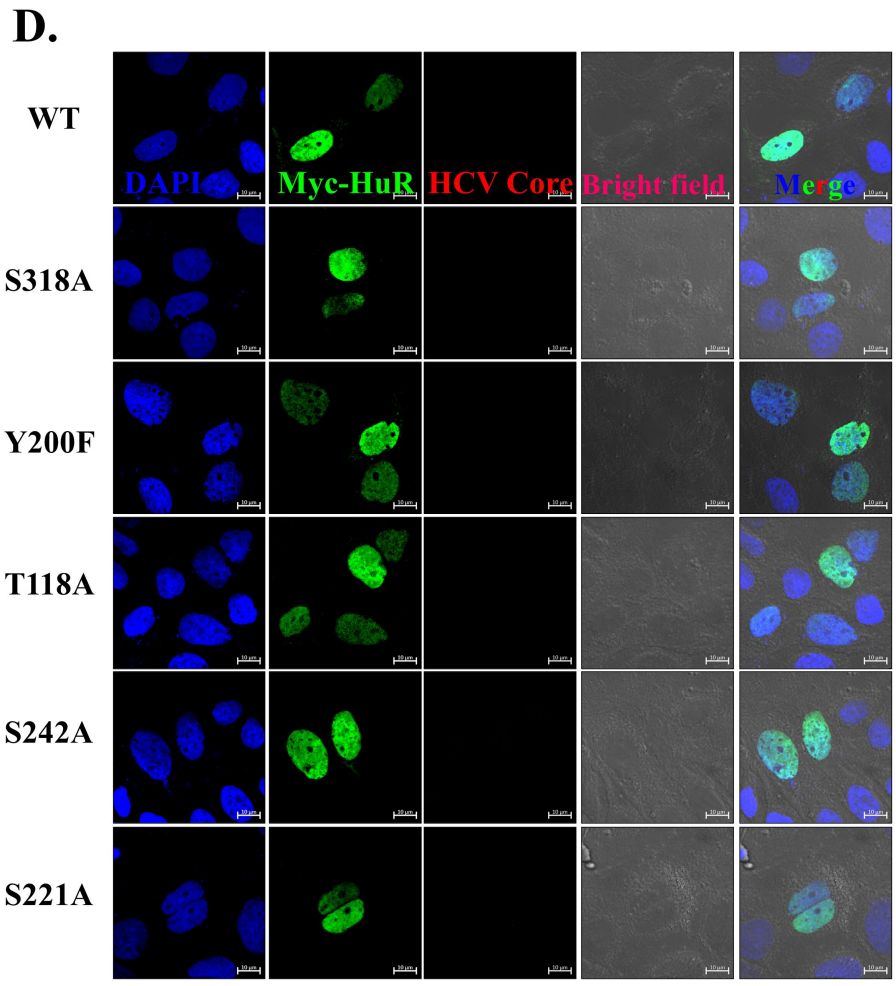
D.
WT
S318A
Y200F
T118A
S242A
S221A
DAPI
Myc-HuR
HCV Core
Bright field
Merge

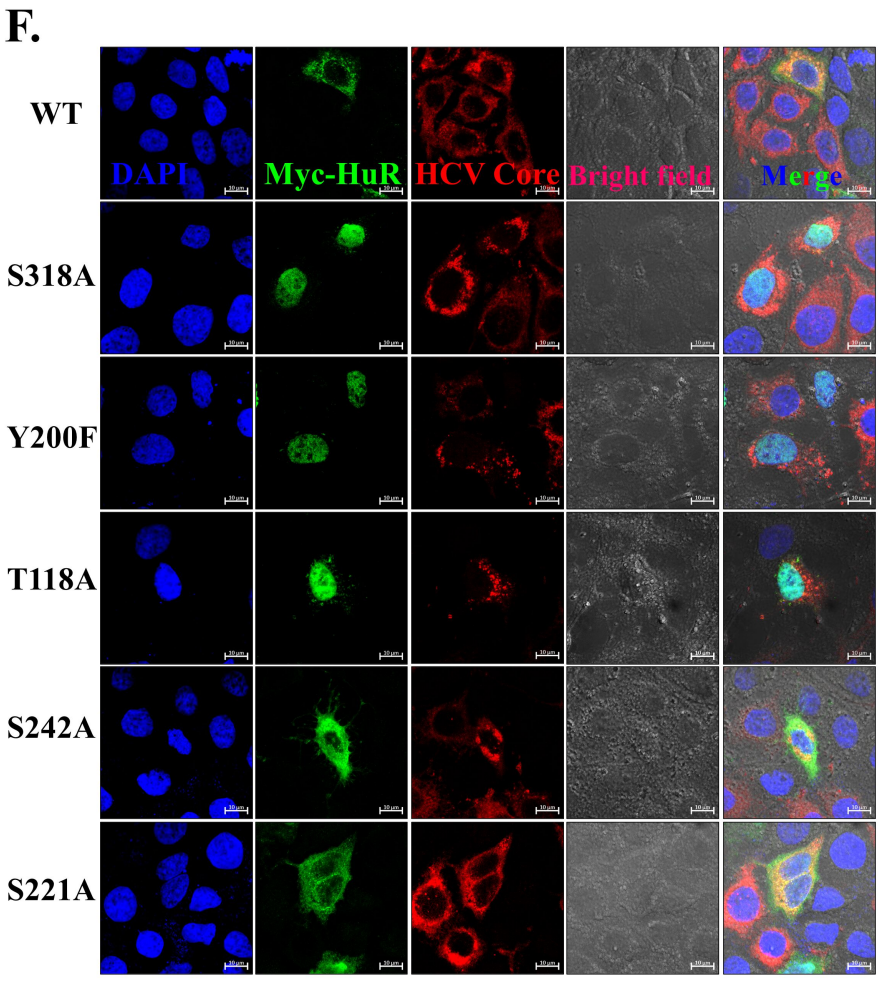
F.
WT
S318A
Y200F
T118A
S242A
S221A
DAPI
Myc-HuR
HCV Core
Bright field
Merge

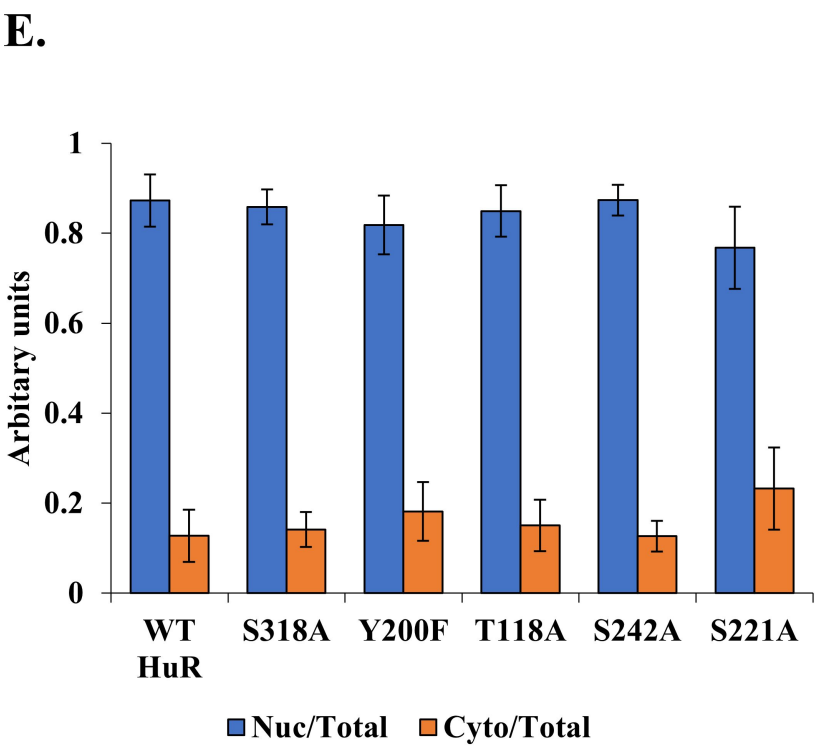
E.
Arbitary units
1
0.8
0.6
0.4
0.2
0
WT HuR
S318A
Y200F
T118A
S242A
S221A
Nuc/Total
Cyto/Total

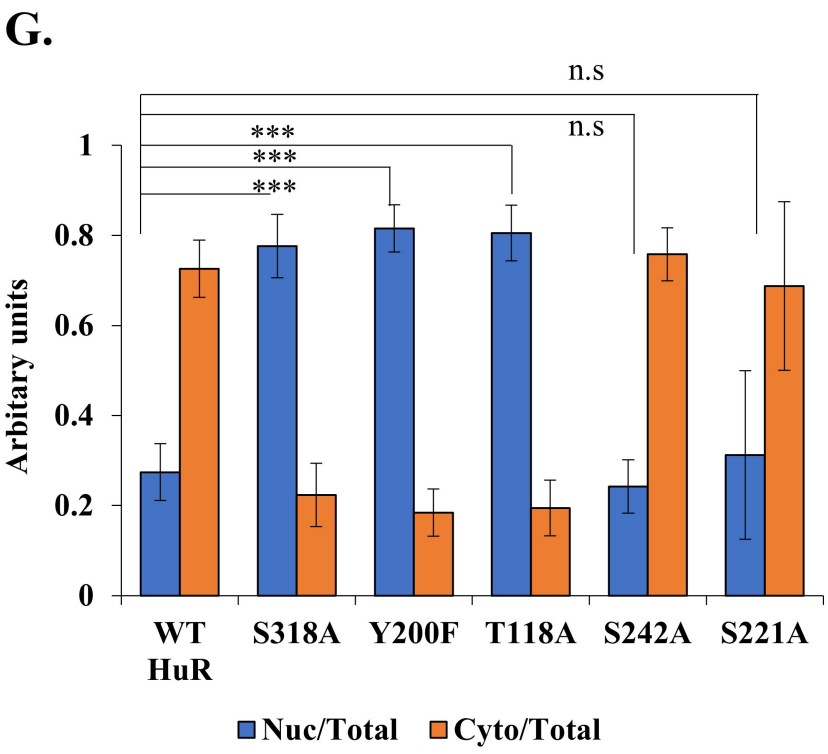
G.
n.s
n.s
***
***
***
Arbitary units
1
0.8
0.6
0.4
0.2
0
WT HuR
S318A
Y200F
T118A
S242A
S221A
Nuc/Total
Cyto/Total

Figure 2.

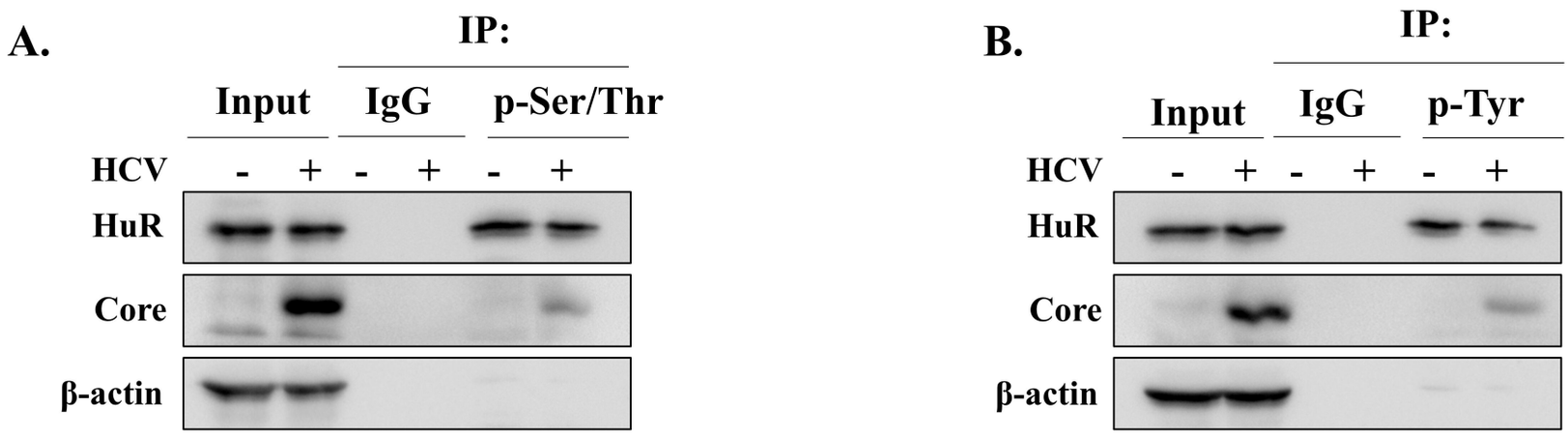
A.
IP:
Input
IgG
p-Ser/Thr
HCV
-
+
-
+
-
+
HuR
Core
β-actin
B.
IP:
Input
IgG
p-Tyr
HCV
-
+
-
+
-
+
HuR
Core
β-actin

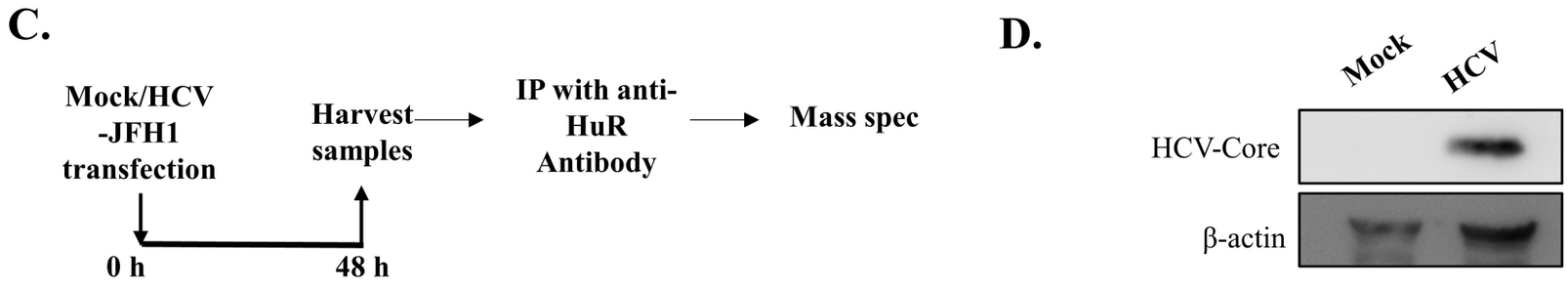
C.
Mock/HCV
-JFH1
transfection
Harvest
samples
IP with anti-
HuR
Antibody
Mass spec
0 h
48 h
D.
Mock
HCV
HCV-Core
β-actin

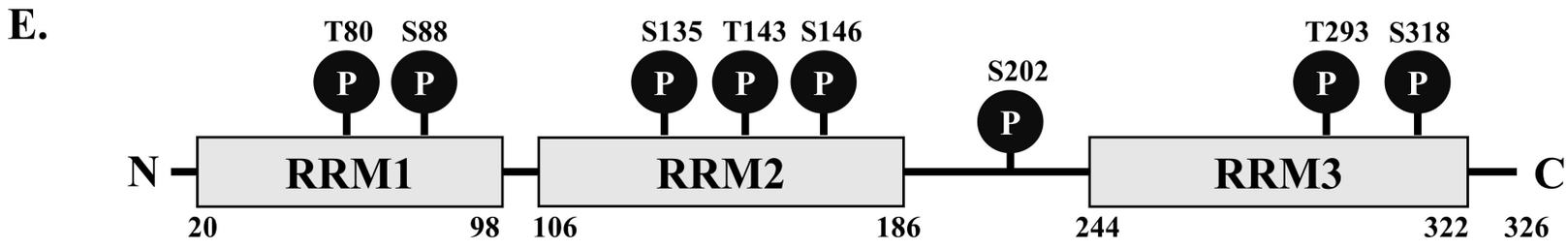
E.
T80
S88
S135
T143
S146
S202
T293
S318
P
N
RRM1
RRM2
RRM3
C
20
98
106
186
244
322
326

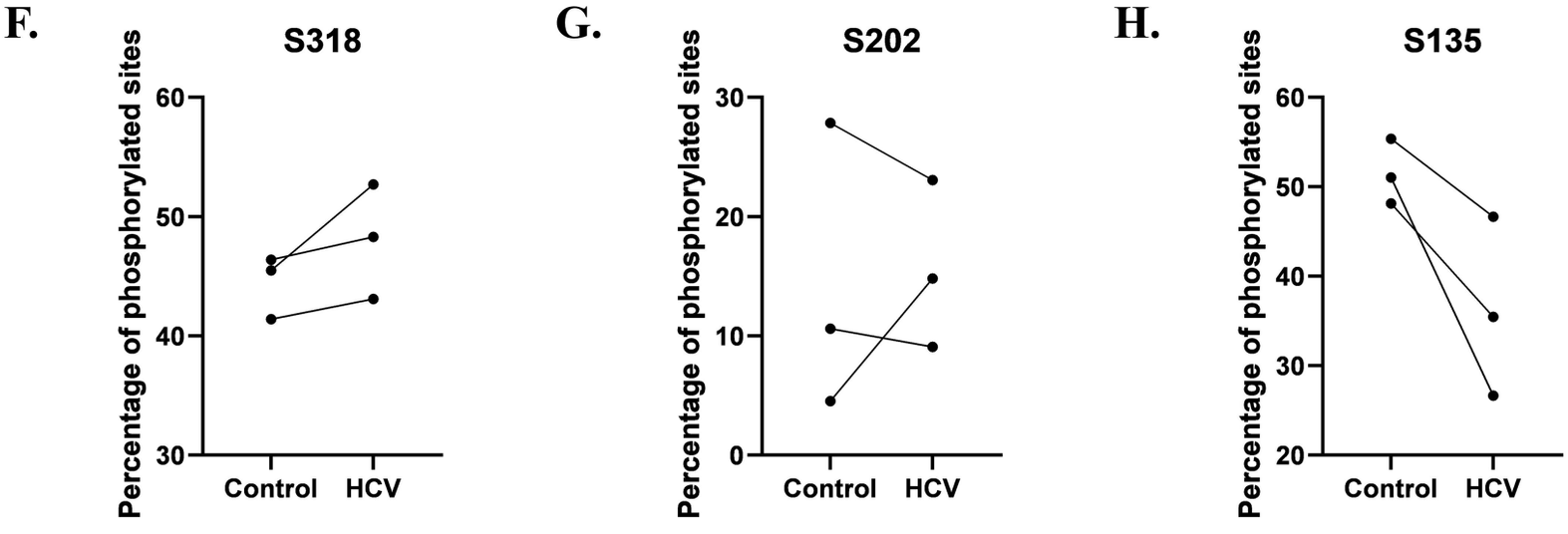
F.
S318
Percentage of phosphorylated sites
60
50
40
30
Control
HCV
G.
S202
Percentage of phosphorylated sites
30
20
10
0
Control
HCV
H.
S135
Percentage of phosphorylated sites
60
50
40
30
20
Control
HCV

Figure 3.

A.

S318 site in HuR RRM3

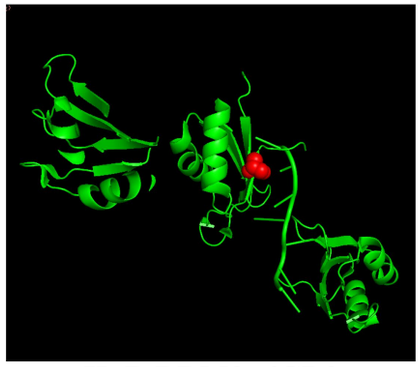

HuR RRM3: 6GD2

E.

Protein	Kd (nM)
WT HuR	25.7 +/- 1.6 nM
S318D HuR	6.36 +/- 2.2 nM
S318A HuR	46.2 +/- 6.2 nM

B.

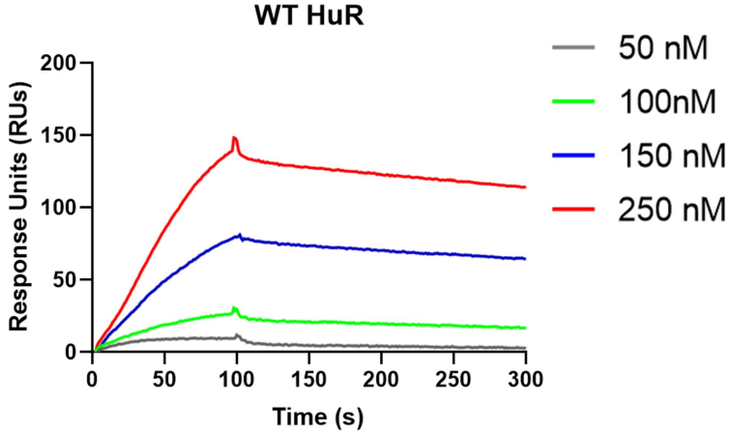

C.

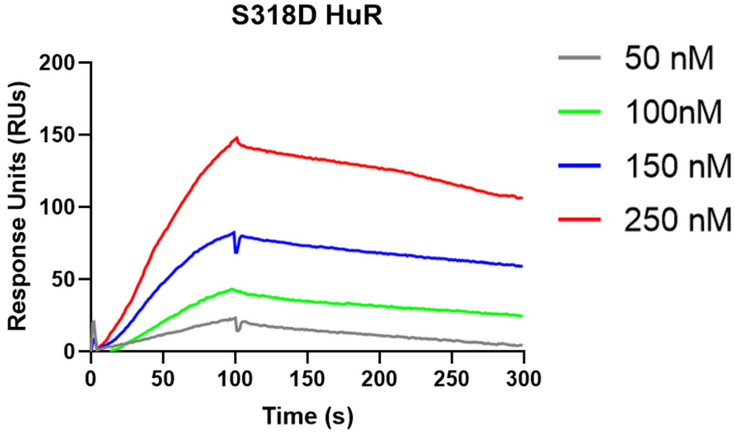

D.

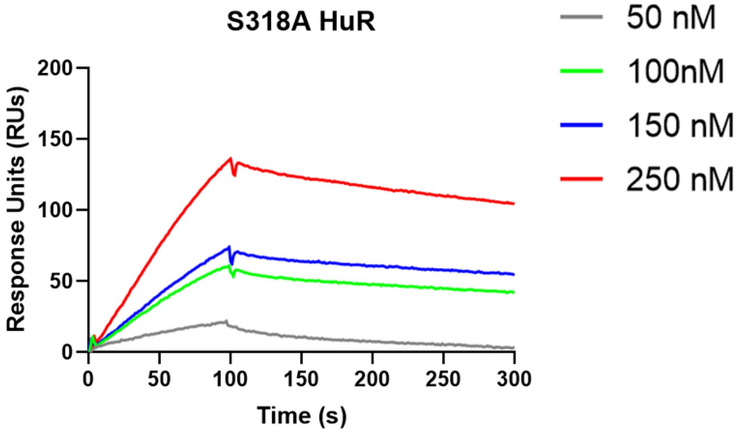

F.

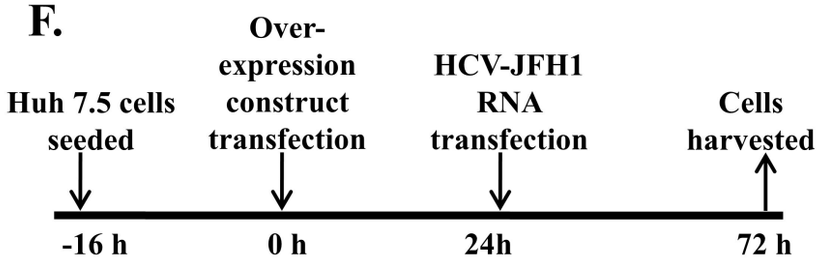

G.

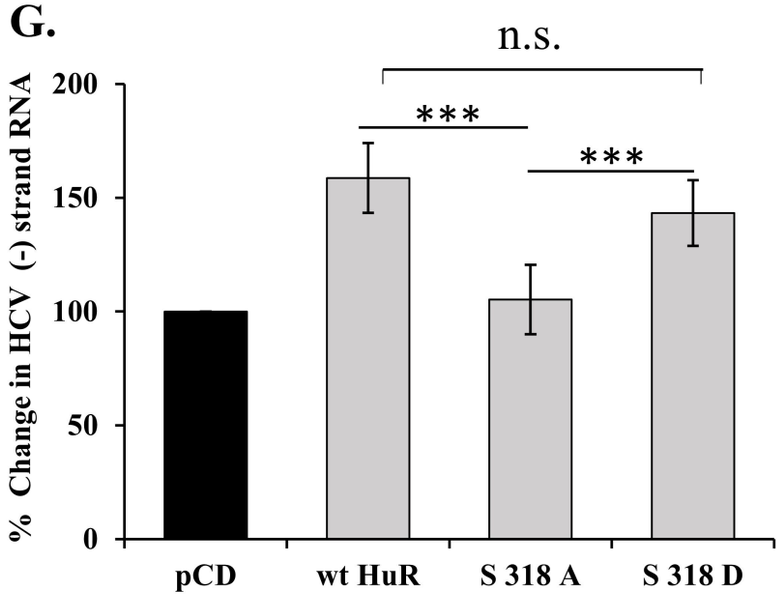

H.

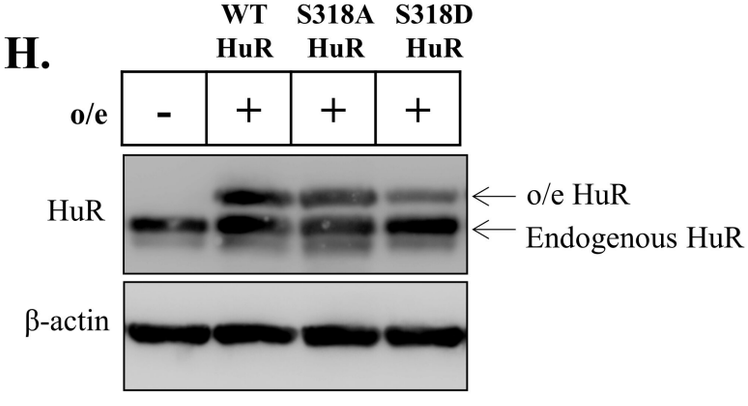

Figure 4.

A.

HuR Phosphorylation Site	Upstream Kinase involved
S318	PKCδ (Doller A et al., Carcinogenesis, 2011)

B.

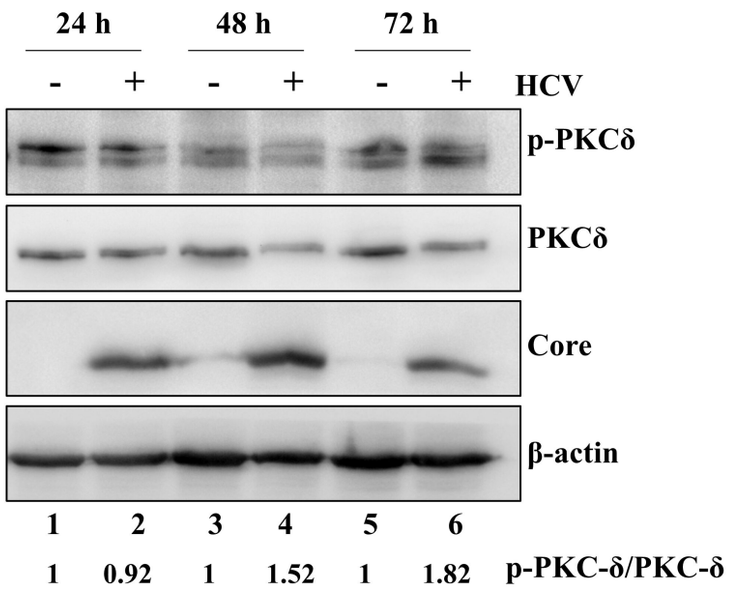

C.

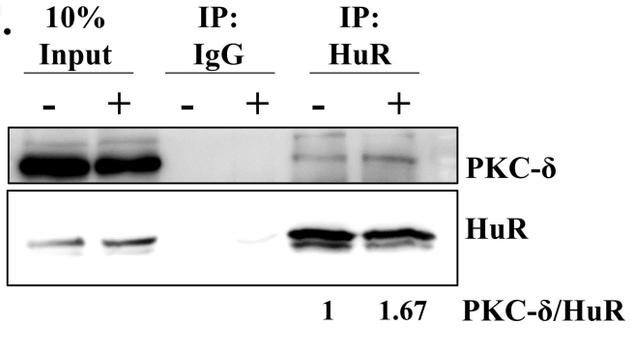

D.

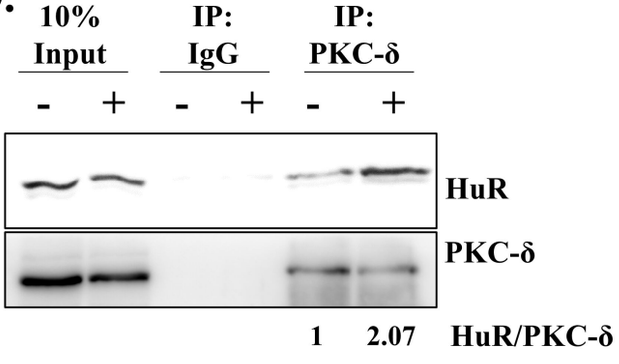

E.

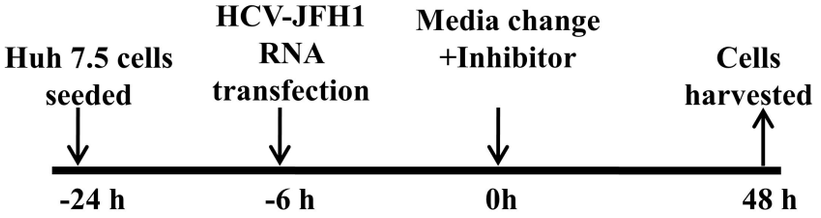

F.

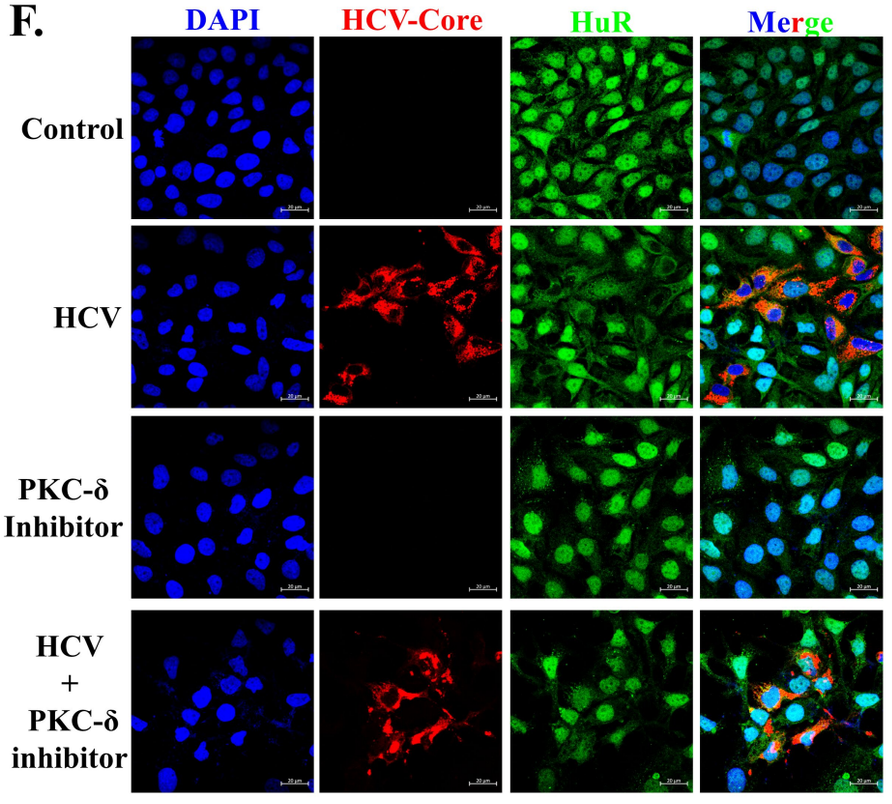

G.

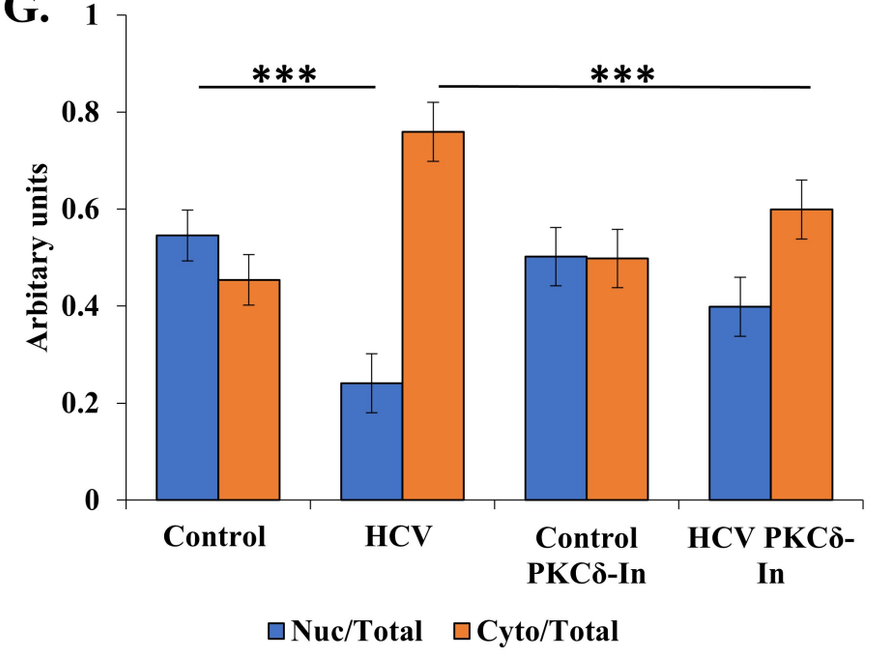

Figure 5.

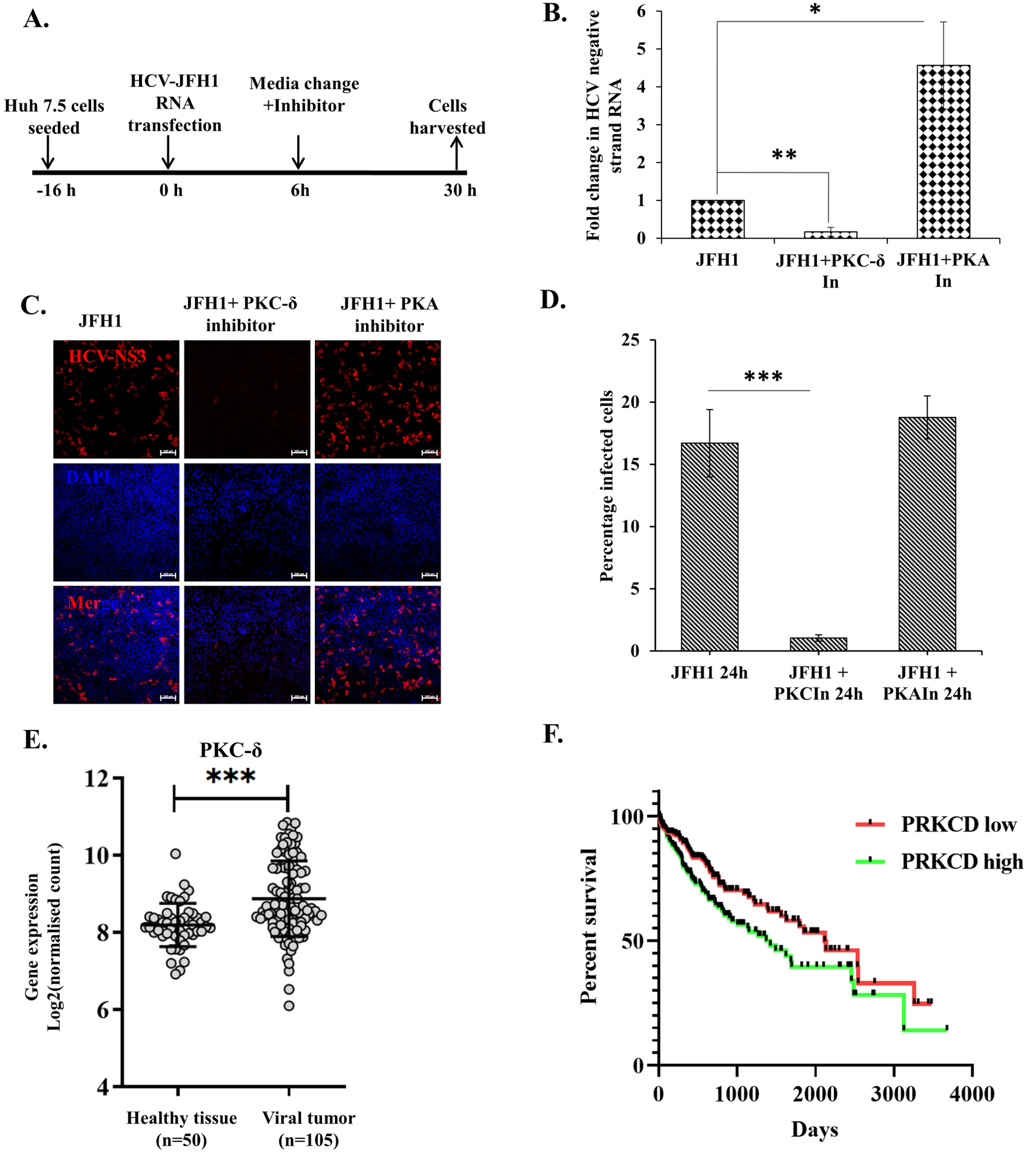
A.
Huh 7.5 cells seeded
HCV-JFH1 RNA transfection
Media change +Inhibitor
Cells harvested
-16 h
0 h
6h
30 h
B.
Fold change in HCV negative strand RNA
*
**
JFH1
JFH1+PKC-δ In
JFH1+PKA In
C.
JFH1
JFH1+ PKC-δ inhibitor
JFH1+ PKA inhibitor
HCV-NS3
DAPI
Merge
D.
Percentage infected cells
***
JFH1 24h
JFH1 + PKCIn 24h
JFH1 + PKAIn 24h
E.
PKC-δ
***
Gene expression Log2(normalised count)
Healthy tissue (n=50)
Viral tumor (n=105)
F.
Percent survival
PRKCD low
PRKCD high
Days

Figure 6.

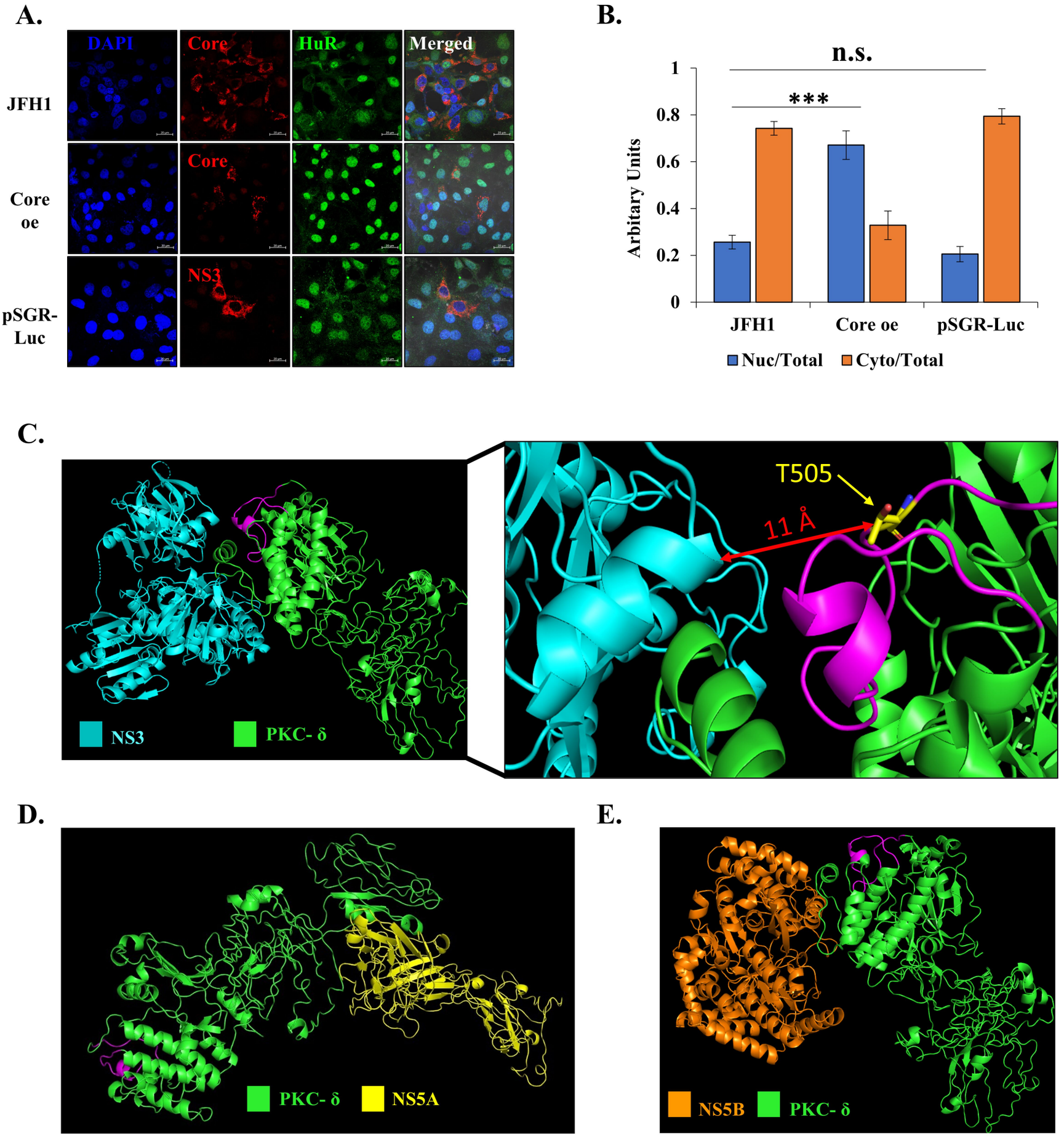
A.
DAPI
Core
HuR
Merged
JFH1
Core oe
Core
pSGR-Luc
NS3
B.
n.s.
***
Arbitary Units
1
0.8
0.6
0.4
0.2
0
JFH1
Core oe
pSGR-Luc
Nuc/Total
Cyto/Total
C.
NS3
PKC- δ
T505
11 Å
D.
PKC- δ
NS5A
E.
NS5B
PKC- δ

Figure 7.

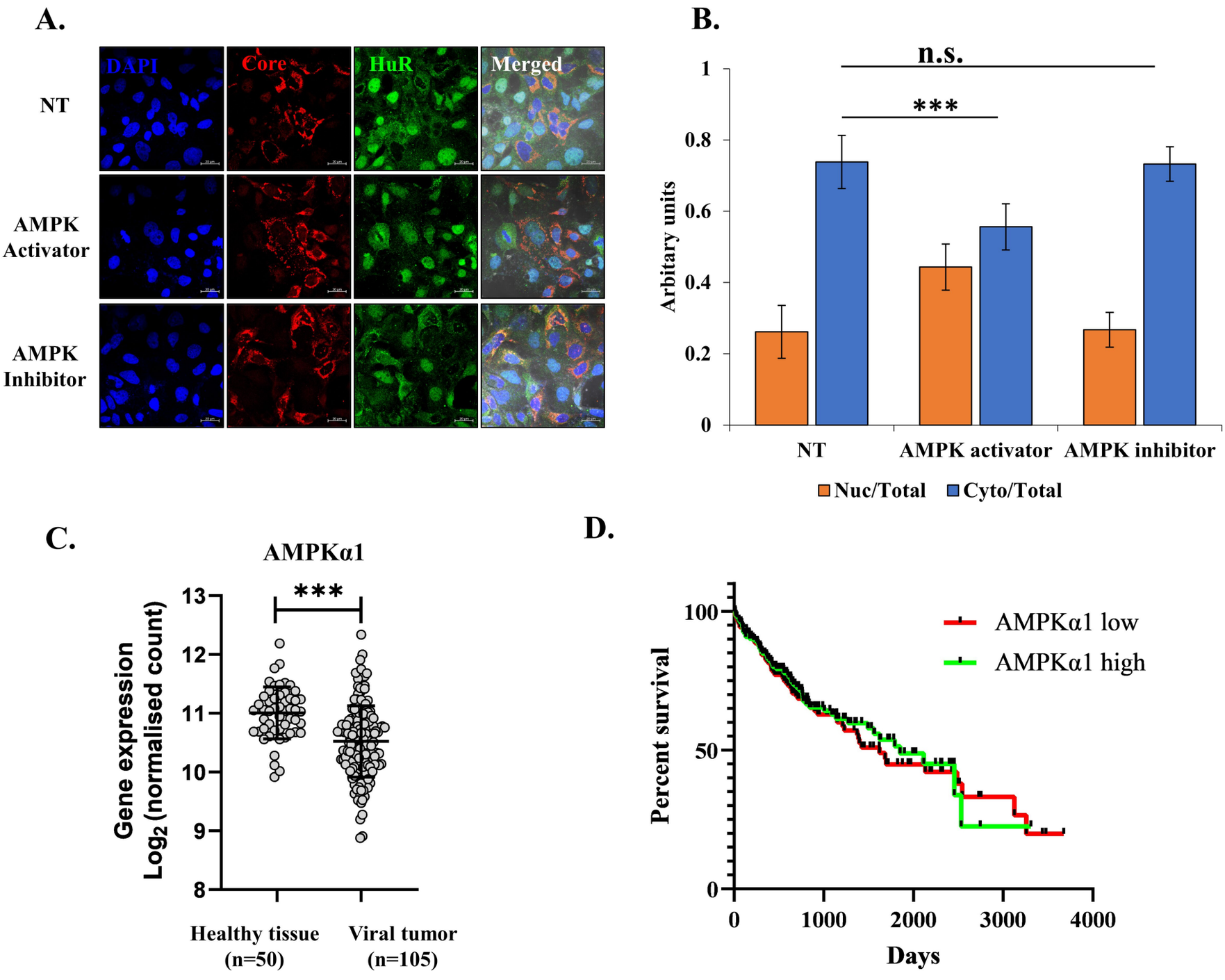
A.
DAPI
Core
HuR
Merged
NT
AMPK Activator
AMPK Inhibitor
B.
n.s.
***
Arbitary units
1
0.8
0.6
0.4
0.2
0
NT
AMPK activator
AMPK inhibitor
Nuc/Total
Cyto/Total
C.
AMPKα1
***
Gene expression
Log2 (normalised count)
13
12
11
10
9
8
Healthy tissue
(n=50)
Viral tumor
(n=105)
D.
AMPKα1 low
AMPKα1 high
Percent survival
100
50
0
0
1000
2000
3000
4000
Days

Figure 8.

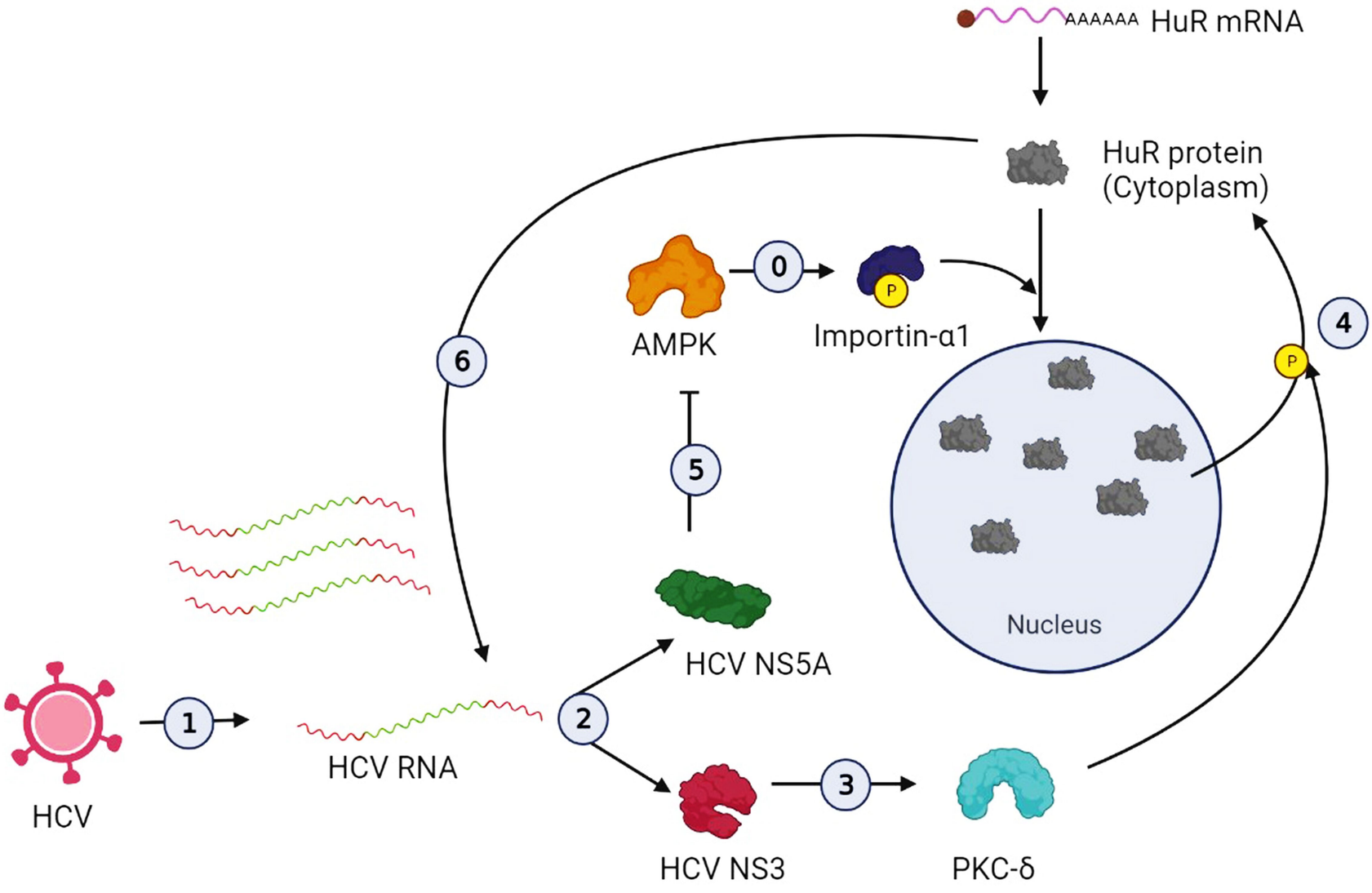
AAAAAA
HuR mRNA
HuR protein
(Cytoplasm)
0
AMPK
P
Importin-α1
4
P
6
5
Nucleus
HCV NS5A
1
HCV
HCV RNA
2
3
HCV NS3
PKC-δ